Universitat Autònoma de Barcelona

CARACTERITZACIÓ I APLICACIÓ DE MEMBRANES DE POLISULFONA I DESENVOLUPAMENT DE NOVES MEMBRANES D'IMPRESSIÓ MOLECULAR

Aleix Conesa Cabeza

Tesi Doctoral
Programa de Doctorat en Química

Directores:
Tània Gumí Caballero
Cristina Palet Ballús

Departament de Química
Facultat de Ciències

2015

CAPÍTOL 4. CONCLUSIONS

4. CONCLUSIONS

Dels estudis realitzats en el present treball en podem concloure de forma global els següents punts més important:

- S'ha pogut crear per primera vegada en el camp de les membranes un nou mètode d'anàlisis que permet distingir les membranes d'inversió de fase segons si han estat preparades per evaporació o per immersió. També permet classificar-les pel seu gruix, només realitzant un simple espectre d'infraroig proper (NIR) de la superfície i aplicant-hi un mètode supervisat de modelatge basat en l'anàlisi de variança residual. Es tracta d'un mètode de classificació per membranes nou, ràpid, econòmic i senzill, que pot ser fàcilment implementat en qualsevol fàbrica de membranes com a control de qualitat.
- Mitjançant la microscòpia electrònica d'escrombrat (SEM) i la microscòpia de força atòmica (AFM) s'ha determinat quin es l'efecte d'algunes de les variables més importants que afecten a la formació dels *macrovoids* durant la preparació de membranes de polisulfona com són el gruix de membrana, la temperatura del bany de coagulació o la presència d'altres compostos químics com l'isopropil miristat. Poder controlar la presencia dels *macrovoids* a l'estructura de les membranes, permet optimitzar la funcionalitat d'aquestes ja que els *macrovoids* poden afectar les propietats fisicoquímiques de la membra com són la seva capacitat de transport, la filtració o la vida útil.
- S'ha demostrat que les membranes de nanofiltració de polisulfona amb una capa de poliamida poden disminuir el Carboni Orgànic Total (TOC) de 500 ppm a 62 ppm d'una solució d'aigua oxigenada al 40 % utilitzant un sistema de filtració frontal. Els estudis realitzats tant a nivell de disminució del TOC com a nivell de caracterització i degradació de els membranes durant el procés de filtració, aporten noves dades experimentals sobre la purificació del peròxid d'hidrogen. Un sector hermètic, tapat per patents i secretisme.
- La preparació de sistemes de reconeixement molecular mitjançant Polímers d'Impressió Molecular (MIP) està molt estesa, en canvi amb sistemes de membrana hi ha menys publicacions. En aquesta memòria s'han preparat i caracteritzat 4 tipus diferents de Membranes d'Impressió Molecular (MIM) per a la separació quiral d'un racèmic de DL-selenometionina, sent la més enantioselectiva de totes la formada pel copolímer N,N-dimetil-2-aminoetilmetacrilat-etilenglicol dimetacrilat (DMAEM-EDMA).

A continuació es descriuen més detalladament les conclusions per a cada un dels treballs realitzats.

Caracterització de membranes polimèriques mitjançant espectroscòpia d'infraroig proper (NIR)

- A partir de l'enregistrament de l'espectre NIR de les membranes i el posterior tractament quimiomètric basat en un primer pretractament dels espectres amb el filtre *Standard Normal Variation* (SNV), seguit del càlcul dels components principals (PC) i finalment aplicant un mètode de reconeixement de pautes, concretament el model SIMCA, s'ha creat i validat un mètode per a identificar si una membrana ha estat preparada per la tècnica d'inversió de fases per immersió o per evaporació.
- De la mateixa manera, s'ha creat i validat un model que permet diferenciar membranes de polisulfona preparades per immersió amb diferents gruixos. Concretament es poden distingir membranes entre 84 i 104 μm amb membranes amb gruixos entre 24 i 72 μm.
- Per contra, no s'ha pogut validar cap model que permeti distingir membranes amb diferents gruixos preparades per evaporació, donat que no hi ha diferències morfològiques significatives entre elles.

Preparació i caracterització de membranes polimèriques activades (CAM) per a la separació enantiomèrica de propranolol

- En sistemes de membrana blanc, és a dir membranes preparades a partir de polisulfona (PSf)/dimetilformamida (DMF)/aigua i emprant el procediment d'inversió de fase per immersió, es formen *macrovoids* a partir d'uns 40 μm de gruix de membrana. A partir d'aquest gruix, els *macrovoids* creixen progressivament. S'ha vist que en el seu procés de creixement a mida que augmenta el gruix de la membrana, els macrovoids primer s'eixamplen i posteriorment s'allarguen.
- En sistemes de membrana amb modificador, en els que s'ha emprat isopropil miristat (IPM), i també preparats per inversió de fase per immersió, en aquest cas els macrovoids tenen forma de dit (*fingerlike*), i les seves dimensions es mantenen pràcticament constants tot i variar el gruix de la membrana.

- En sistemes de membrana amb modificador i agent transportador, en aquest cas N-hexadecil-L-hidroxiprolina (HHP), el comportament és similar a l'anterior, donat que el reactiu HHP s'incorpora a baixes concentracions.
- Tornant als sistemes de membrana blanc (PSf/DMF/aigua), l'increment de temperatura del bany de coagulació de 4 a 40ºC no influeix en la morfologia dels macrovoids. En canvi, pels sistemes (PSF+IPM)/DMF/aigua i (PSF+IPM+HHP)/DMF/aigua la variació de la temperatura del bany sí que provoca variacions en la morfologia de la membrana. De manera que, en augmentar la temperatura s'observa una disminució de la presència de *macrovoids*.
- L'increment de la concentració d'IPM en els sistemes de membrana amb aquest modificador (PSf+IPM)/DMF/aigua, repercuteix amb un augment de la quantitat dels macrovoids en forma de dit, la qual cosa emfatitza el paper d'aquest compost en la morfologia de la membrana.
- Amb les anàlisis de microscòpia de força atòmica (AFM) s'ha comprovat que la presència d'IPM i/o HHP no afecta significativament a la rugositat superficial de les membranes preparades per inversió de fase i immersió (DMF/aigua), ni tampoc a la mida mitjana de porus. Per contra, s'observa una disminució considerable de la rugositat quan s'utilitza cloroform/metanol com a parell solvent/no solvent, o bé, quan la tècnica de preparació emprada es també per inversió de fases per evaporació.
- Les membranes corresponents al sistema amb modificador, (PSf+IPM)/DMF/aigua, preparades per immersió presenten transport no enantioselectiu, el qual correspon a un transport per difusió dels enantiòmers del propranolol a través de la membrana. En canvi amb les membranes que contenen l'agent transportador HHP s'observa certa enantioseparació, tal i com era d'esperar.

Eliminació de compostos orgànics d'aigua oxigenada al 40% mitjançant membranes polimèriques

- Les membranes comercials tant de nanofiltració com d'osmosis inversa de polisulfona i amb una capa de poliamida procedents de les cases comercials *Dow*, *Hydranautics* y *GEOsmotics* presenten una bona resistència química y

mecànica tant a l'exposició d'aigua oxigenada al 40% durant una setmana, com quan són emprades en un sistema de filtració frontal sota una pressió de 5 bars.

- En el cas de la membrana d'osmosis inversa d'acetat de cel·lulosa de la casa comercial *GEOsmotics* s'observa una gran degradació tant a l'exposició com a la filtració amb l'agua oxigenada al 40%.
- Concretament, les membranes de nanofiltració de polisulfona ESPA1 i CPA2, de la casa comercial *Hydranautics*, permeten una disminució de TOC de 500 ppm fins a 67 i 87 ppm respectivament, quan s'aplica successivament una doble filtració frontal a un volum de 10 ml de solució.

Preparació, caracterització i aplicació de membranes d'impressió molecular (MIM) per a la separació quiral de L,D-selenometionina

- S'han preparat membranes d'impressió molecular sobre suport de PVDF amb els monòmers 4-vinilpiridina (4VPY), àcid metacrílic (MAA), acrilamida (AM) i N,N-dimetil-2-aminoetilmetracrilat (DMAEM), copolimeritzats amb l'etilenglicol dimetacrilat (EDMA) i emprant benzoïl èter com iniciador i llum ultraviolada.
- Mitjançant el càlcul del grau de modificació (DM) s'ha determinat que, amb un temps màxim de 3 hores els polímers d'impressió queden totalment dipositats sobre la membrana.
- Amb unes condicions de pH 8 i utilitzant un sistema de separació per diàlisis, s'ha comprovat que dels 4 tipus de membrana preparades, la formada per AM no té capacitat de separació quiral, mentre que amb les formades per 4-VPY, MAA i DMAEM s'ha aconseguit un factor de separació α de 1,18 ± 0,05, 1,20 ± 0,06 i 1,37 ± 0,09 respectivament.
- S'ha comprovat que la membrana d'impressió molecular formada per DMAEM-EDMA, la que ofereix major separació quiral es forma correctament sobre el suport de PVDF utilitzant diferents tècniques de caracterització com són el FTIR-ATR, SEM-EDS, 13C CP/MAS NMR.
- S'ha comprovat mitjançant ICP-MS que el procés d'extracció de la molècula L-selenometionina utilitzada com a molècula patró per a la síntesi i preparació de la membrana d'impressió molecular (MIM) és total i completa, i que per tant la MIM queda lliure d'aquesta.

- La millor separació quiral d'una solució del racèmic DL-selenometionina, en un sistema de filtració per diàlisis, s'ha obtingut amb la membrana d'impressió molecular preparada amb el monòmer DMAEM i l'entrecreuador EDMA ajustant el pH de les solucions aquoses de càrrega y receptora a 6, aconseguint un factor de separació α de 1,75±0,12.

ANNEX 1

Available online at www.sciencedirect.com
ScienceDirect
Journal of Membrane Science 300 (2007) 122–130
journal of MEMBRANE SCIENCE
www.elsevier.com/locate/memsci

Near infrared spectroscopy: A novel technique for classifying and characterizing polysulfone membranes

A. Conesa [a], T. Gumí [b], J. Coello [c], C. Palet [a,*]

[a] Centre Grup de Tècniques de Separació en Química, Departament de Química, Universitat Autònoma de Barcelona, 08193 Bellaterra, Catalunya, Spain
[b] Institut Européen des Membranes, IEM/UMII, Place Eugène Bataillon, CC 047, 34095 Montpellier, Cedex 5, France
[c] Grup de Quimiometria Aplicada, Departament de Química, Universitat Autònoma de Barcelona, 08193 Bellaterra, Catalunya, Spain

Received 15 December 2006; received in revised form 14 May 2007; accepted 15 May 2007
Available online 29 May 2007

Abstract

The industrial manufacture of membranes is well established at the present time. More than any other process, the production of ultrafiltration membranes by immersion or evaporation (phase inversion) precipitation techniques is one of the most common. In many cases, the macroscopic properties of the membranes are similar from one membrane to another and it is impossible to distinguish them, while they differ notably from the microscopic point of view. The aim of this work is to develop a method for the classification of polysulfone ultrafiltration membranes prepared either by immersion or evaporation. It also presents a classification of those membranes by thickness. For these purposes, near infrared spectroscopy (NIR) combined with chemometric techniques are attempted here for the first time in the area of membrane research. The NIR technique permits fast analytical measurement of membrane samples, together with the possibility of characterization in on-line mode, without destruction or invasion of the samples. This appears to be an excellent routine analysis for purposes of membrane classification. The membranes were prepared in our *Universitat Autònoma de Barcelona* (*UAB*) laboratory and, after obtaining the NIR spectra, principal component analysis (PCA) was used to describe the system. The second stage involved the application of a pattern recognition method: supervised independent modeling of class analogy (SIMCA) in order to classify unknown samples. Finally, the ultrafiltration membranes were classified in terms of the membrane preparation technique (immersion or evaporation). In addition, membranes prepared by immersion were classified by thickness.

Keywords: NIR; Membrane classification; Membrane characterization; Polysulfone membrane

1. Introduction

In recent decades, membrane technology has become a common separation technique. The main attraction of membrane technology is that it consumes a relatively low amount of energy and involves a simple and well-arranged set-up process. There are four types of membrane filtration, ultrafiltration, microfiltration, nanofiltration and reverse osmosis. Membrane filtration can be used as an alternative for flocculation [1] sediment purification [2] adsorption (sand filters and active carbon filters, ion exchangers), extraction [3,4] and distillation [5]. Whatever the application or filtration envisaged, it is very important to know such membrane properties as; porosity, water permeation flux, mechanical resistance, etc. Therefore, the characterization of the membrane becomes compulsory in order to guarantee the correct application of membrane technology [6].

Polymeric membranes have different features depending on the preparation technique employed. There are also other parameters that influence the morphology, such as the polymer concentration [7] the selection of the solvent/nonsolvent pair [8] the membrane thickness [9–11] the presence of additives [12] the temperature of the coagulation bath [13] or the presence of certain solvents [14] among others.

Nowadays there are many techniques for physically characterizing membranes [15]. We can use them to determine their structural and morphological properties. For example, such microscopy techniques as scanning electron microscopy (SEM) or atomic force microscopy (AFM) [16,17]; liquid penetration methods, such as liquid displacement or the mercury intrusion method, as well as techniques based on gas/liquid adsorption and desorption such as permporosimetry.

* Corresponding author. Tel.: +34 935813475; fax: +34 935812379.
E-mail address: cristina.palet@uab.cat (C. Palet).

0376-7388/$ – see front matter © 2007 Elsevier B.V. All rights reserved.
doi:10.1016/j.memsci.2007.05.020

This work considers, for the first time in membrane characterization, the use of a well-known technique, which is able to analyze the morphological and chemical structure of certain ultrafiltration membranes: near infrared spectroscopy (NIR) combined with chemometric techniques. This technique is already applied to a wide variety of fields including the food [18], pharmaceutical [19], medical [20,21] and petrochemical [22] industries. NIR spectra consist of overtones and combinations of fundamental vibration bands in the mid infrared region (3000–1700 cm^{-1}). The bonds involved are generally C–H, N–H and O–H [23]. The characteristics of the absorption bands in NIR spectra depend on both the chemical composition and the physical properties of samples, such as crystallinity, crystal shape, polymorphism and particle size [24,25]. An important element of the feasibility of NIR spectroscopy is that neither pretreatment of samples, nor destructive or invasive techniques are necessary. One of the interesting possibilities of NIR is its use as a quality control technique, whereby it can be used to make measurements in on-line mode as a very fast form of routine analysis.

After the preparation and storage of membranes, it may indeed be necessary for them to be classified, as is the case with most membranes manufactured today: microfiltration, nanofiltration and reverse osmosis membranes. In order to avoid any possible mistakes, a membrane sample can be analyzed by NIR and immediately after, the right chemometric software may help for it to be classified, if certain known membranes have been prepared previously as patterns or standards.

In this work, we assessed the use of NIR spectrometry combined with chemometric techniques to develop a calibration model, which could determine or predict the membrane preparation technique used, as well as the membrane thickness obtained. Principal component analysis (PCA) is used to describe the system and the supervised independent modeling of class analogy SIMCA [26] classification is used to obtain the classification model.

2. Experimental

2.1. Materials

Non-woven fabric (Hollytex 3329) was used as a mechanical support for the membranes. The polysulfone (PSf) used in this study was supplied by BASF (Barcelona, Spain) under the trade name of Ultrason S3010 incolor. The solvent/nonsolvent pair employed was *N*-dimethylformamide (DMF) (Sigma–Aldrich, Germany)/distilled water.

2.2. Membrane preparation

Polysulfone was dissolved in DMF to a concentration of 13 wt.%. Then, the PSf solution was spread using a casting knife on the non-woven fabric surface that was supported on a glass plate. Membranes of thickness between 22 and 115 μm were properly obtained by performing two different membrane preparation procedures. In the case of phase inversion precipitation by immersion, the nascent membranes were immediately, after casting, immersed in a coagulation bath, together with the glass plate, where they were left for a minimum of 30 min. The temperature of the coagulation bath was fixed at 4 °C. Later, the membranes were washed and stored in water until analysis [15]. When performing membrane precipitation by evaporation, the solvent is left to evaporate at room temperature in an environment of 40% relative humidity, and membranes were then dry-stored.

Different membranes were prepared on different days, weeks and months in order to consider the reproducibility of such membrane preparation techniques. A minimum of two replicates were prepared each time in order to evaluate repetitively.

2.3. Recording of NIR spectra

NIR spectra were recorded on a FOSS NIRSystems 6500 spectrophotometer. The instrument was controlled via the software Vision 2.55, also from NIRSystem, which permits acquisition and processing of spectra. To improve the quality of the spectra, in terms of scattering reduction, standard normal variate (SNV) pre-treatment was applied. Qualitative analyses were conducted using the Software Unscrambler V9.1, from CAMO A/S that permits the use of supervised independent modeling of class analogy (SIMCA).

Spectra were recorded in reflectance mode. Membrane samples area was of 0.2 cm^2. Each spectrum was recorded at least twice, with an average of 32 scans performed at 2 nm intervals for each one over the wavelength range of 1100–2500 nm.

A total of 150 membrane samples, with three different thicknesses, were prepared (by the aforementioned two membrane preparation techniques). Half of them were prepared by the immersion technique and other 75 by evaporation. In the case of the immersion technique, 26 membranes of a thickness of 26 μm (namely class A), 25 membranes of a thickness of 61 μm (namely class B), and 24 membranes of a thickness of 95 μm (namely class C) were obtained. For the evaporation technique, 24 membrane samples of a thickness of 46 μm (class A), 24 membranes of a thickness of 68 μm (class B), and 27 membranes of a thickness of 93 μm (class C) were prepared. In all cases, the given thickness value corresponds to the average thickness measurements of all the membranes in a group.

2.4. Scanning electron microscopy (SEM) analysis

The cross-section images of the prepared membranes were obtained by scanning electron microscopy (SEM), Hitachi H-7000 (Hitachi Ltd., Japan, Tokyo). To do this, membrane samples were submerged in ethanol, then frozen in liquid nitrogen and fractured. After coating with gold, they were transferred to the microscope.

2.5. Data processing

To facilitate the interpretation of the analytical information obtained from the membrane NIR spectra data, the principal component analysis (PCA) was calculated and then a pattern recognition method [27] was applied. PCA was first formulated

in statistics by Pearson [28]; since then, the utility of PCA in many diverse scientific fields has been discovered as a technique for reducing the amount of data and to eliminate their correlation. Details about different mathematical methods to extract the principal components may be found in [29].

For m samples, their spectra are ordered in a matrix X with m rows, termed "objects" (in this case the samples) and p columns, termed "variables" (in this case wavelengths values). Statistically, PCA may be viewed as an expansion of X in as many components as min (m, p); this corresponds to expressing X in a new coordinate system. The success on the use of PCA comes when this statistic approach is slightly changed and PCA is viewed as the approximation of the original data matrix X by a product of two small matrices (the score and loading matrices) according to

$$X = TL' + E \tag{1}$$

where T is the scores matrix with m rows and r columns (number of principal components); L' is the transpose loading matrix with r rows and p columns. E is the residuals matrix. The basic assumption in the use of PCA is that the score and loading vectors corresponding to the first principal components contain the most useful information relating to the specific problem, and that the remaining ones mainly comprise noise. Therefore, these vectors are usually written in order of descending eigenvalues, and only the first r are retained. Several criterions to decide the number of principal components retained, r, may be found in the literature [30].

Mathematically, the projection of X down on to a r-dimensional subspace by means of the projection matrix L' gives the sample coordinates in this plane T. The columns in T are the score vectors for each principal component, and give us information about the samples. The rows in L' are called loading vectors, for each principal component, and give us information about the variables.

A residual variance analysis in the principal component space was used to classify samples according to the membrane preparation technique and the corresponding thickness of the obtained membranes. The aim of the analysis was to be able to predict which category a new sample belongs to. The classification method used was the "Soft independent modeling of class analogy" (SIMCA), as indicated [31,32]. SIMCA is a technique that uses PCA for classification. Each class q is modeled by a separate PCA analysis and might reveal a different number of significant principal components.

For a single x-observation

$$x_{ij}^q = \bar{x}_j^q + \sum_{a=1}^{r_q} t_{ia}^q l_{ja}^q + e_{ij}^q \tag{2}$$

where $\bar{x}_j^q$ is the mean of variable j in class q; r_q the number of significant principal components in class q; t_{ia}^q the score of object i on component a in class q; l_{ja}^q the loading of variable j on principal component a in class q and e_{ij}^q is the residual error of object i and variable j in class q.

From the residuals of the samples in the calibration set, a confidence region for the class is constructed around the principal component. New objects are regarded as a member of the class if their distance from the principal component space does not exceed a critical limit defined by the confidence region.

Based on the residual variance of the objects in the calibration set for the class, the residual standard deviation (S) of class q is calculated. Using centered data and when the number of samples in the calibration set of the class, m_q, is less than the number of variables, p_q,

$$S = \sqrt{\frac{\sum_{i=1}^{m_q}\sum_{j=1}^{p_q}(e_{ij}^q)^2}{(m_q - 1 - r_q)(m_q - r_q - 1)}} \tag{3}$$

where e_{ij}^q is the residual of object i in the calibration set at variable j in class q and r_q is the number of significant principal components in class q.

A confidence limit is obtained by defining a critical value of the distance to the model. This is given by

$$S_{\text{crit}} = \sqrt{F_{\text{crit}} S} \tag{4}$$

F_{crit} is the tabulated one-sided value for $(m_q - 1 - r_q)$ and $(m_q - 1 - r_q)$ times $(m_q - r_q - 1)$ degrees of freedom. The S_{crit} is used to calculate the boundary around the model.

The residual standard deviation (S_i) for an object in the calibration set for the class q, when $m_q \leq p_q$ is given by

$$S_i = \sqrt{\frac{\sum_{j=1}^{p_q}(e_{ij}^q)^2}{m_q - 1 - r_q}} \tag{5}$$

Object with $S_i < S_{\text{crit}}$ belongs to the class, otherwise not.

2.6. Calibration set and validation models

The models for each class are calculated using a specified number of principal components and a critical distance with a significance level of 0.05. The optimal number of PCs selected was based on the residual variance curve. This selects the first local minimum unless later PCs give significantly lower residual variance. The results are represented by Cooman's plot [33] where the sample-to-model distances (S_i) are plotted against each other for the two models. This includes class membership limits for both models, so you can see whether a sample is likely to belong to one class, both, or none. If the samples are near the axis, they belong to one class, or could belong to both classes when the samples are near the origin. Outlier samples are those far from the axis.

For each class and at random, certain samples were used as the calibration set, and the remainder to validate the model.

3. Results and discussion

3.1. Membrane thickness characterization by SEM

The casting knife used to prepare the membranes permits the preparation of ultrafiltration membranes of three different

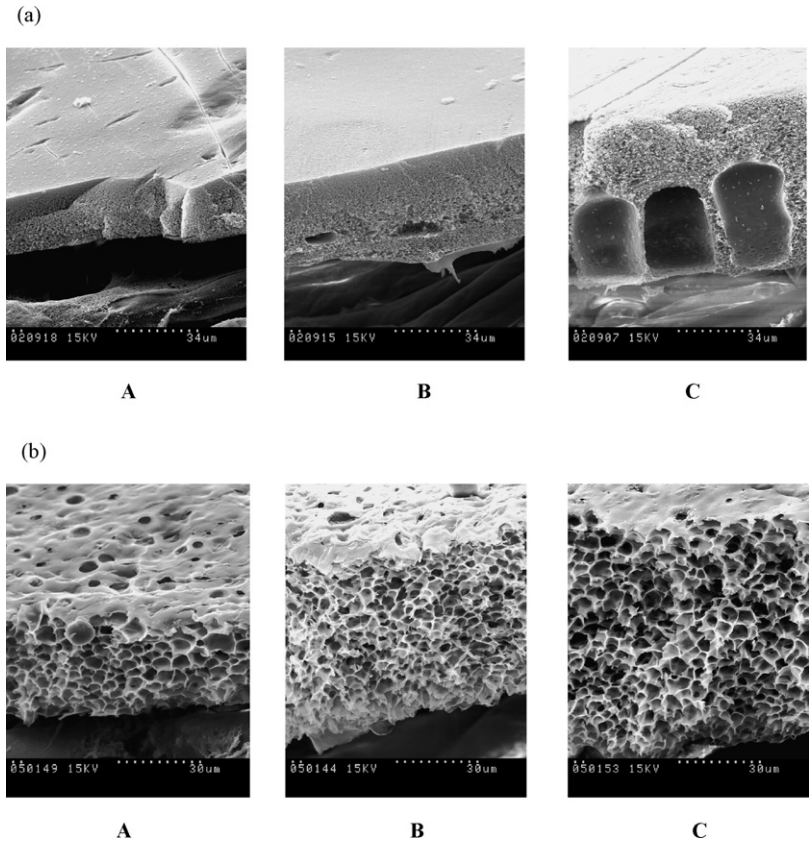

Fig. 1. Cross-section SEM images of the polysulfone ultrafiltration membranes prepared by (a) immersion, or (b) evaporation techniques. Different membrane thicknesses are shown here: immersion technique (A) 26, (B) 61, and (C) 95 μm; evaporation technique (A) 46, (B) 65, and (C) 93 μm.

thicknesses. Fig. 1 shows the SEM cross-section images of various membranes of different thicknesses. Membrane thicknesses were determined (for A, B and C groups, and for immersion and evaporation preparation techniques), as the mean value of all corresponding SEM images of membranes of the same thickness. These values are collected in Table 1.

As we can see, all type A membranes are of a similar thickness even though they are prepared by different phase inversion precipitation techniques (immersion or evaporation). In the case of type B and C membranes, both are slightly thicker when prepared by the evaporation technique. Nevertheless, the most important differences are found in the morphology as shown by the images in Fig. 1. Whereas the membranes prepared by the evaporation technique are all homogeneous, symmetric and similar to each other, the membranes prepared by the immersion technique present more asymmetry (as can be seen in Fig. 1). In the latter case, as the membrane thickness increases, membranes are more asymmetric and macrovoid structures appear.

Table 1
Thickness values obtained (in μm) for membranes prepared by the evaporation or immersion technique

	Evaporation	Immersion
Membranes type A	36–55	24–28
Membranes type B	65–71	49–72
Membranes type C	78–107	85–104

It is known that this phenomenon occurs due to the demixing process that takes place instantaneously when the organic membrane film is immersed in the water coagulation bath, as is the case with the immersion technique procedure [15]. In the former case, when phase inversion takes place after a considerable delay, which is the case with the evaporation technique procedure, the obtained membranes are dense, symmetric and do not give rise to macrovoid formation. A deeper research of polysulfone membrane characterization was doing by Conesa et al. [11].

3.2. NIR Spectra and pre-treatment

The NIR spectra of the total of 150 membranes prepared, as indicated in Section 2, were registered and properly treated. Fig. 2 shows the typical NIR spectrum corresponding to both preparation techniques (immersion and evaporation) and to the different thicknesses or classes (A, B and C).

The most frequent bands in the NIR region correspond to bonds that content atoms with different molecular weight what leads to an increase of the anharmonicity of the bond. Some examples of typical bonds observed in NIR are C–H, N–H or O–H. Depending on the region of wavelengths we can find three general regions in the NIR absorption range: (a) between 1100 and 1700 belonging to the second overtone region; (b) between 1500 and 2000 corresponding to the first overtone region; and (c) finally, the region between 1900–2500 belongs to the com-

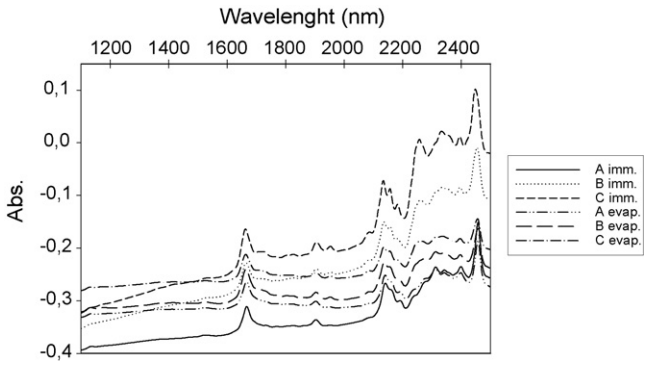

Fig. 2. NIR spectra of the three membrane types (A, B and C of different thicknesses) prepared either by the immersion (imm.) or evaporation (evap.) technique (region extended from 2100 to 2500 nm).

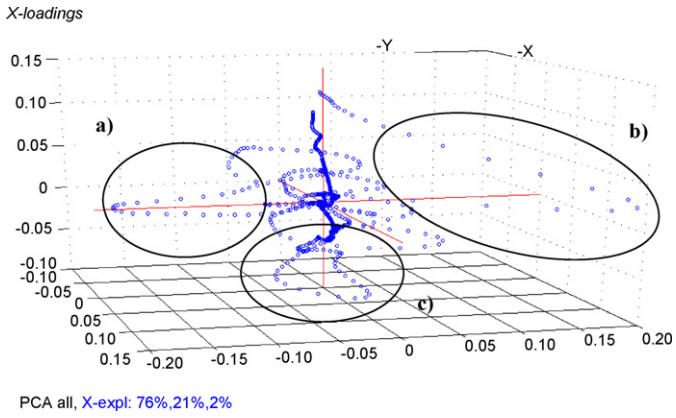

Fig. 3. Loadings plot for the first three PC of all the membranes. Three different areas are formed: (a) 1684–1714 nm; (b) 2274–2444 nm; (c) 2452–2500 nm.

bination band region. The overtones are detected in a frequency twice or three times bigger than the fundamental band, and the combination bands take place when a photon is exiting simultaneously two vibration mode. Therefore, the bands of NIR spectra are of low intensity.

As can be seen in Fig. 2, from 1100 to 1600 nm any spectrum presents bands. However, from 1600 to 2500 nm, the spectra present different band intensities but little differences among them. So, in the spectra of Fig. 2 we can assign the principal functional groups of polysulfone: at 1670 nm the first overtone of the aromatic group; at ca. 2150 the R–OH group of the terminal polymer chain, also corresponding to the first overtone; between 2200 and 2500 nm there are the combination bond bands of C–H/C–H and C–H/C–C; and finally the band of the water at 1900–1950 nm. The different intensity of peaks is basically related to scattering [34] which is a kind of spectroscopic phenomena caused by light being deflected by collisions with other particles. On the order hand, although the little differences do not seem significant at first glance, with the chemometric techniques used, it has been possible to classify the spectra and distinguish them between each other, according to the differences mentioned above.

Those spectra were conveniently pre-treated to improve their quality. In general, as in the present case, the main purpose of these pre-treatments is to reduce the information that is not associated to the property studied, such as displacements of baseline, spectrum noise, scattering, etc. In our case we selected the standard normal variate (SNV) [35], commonly used to reduce scattering. The improved NIR spectra are calculated in accordance with the following formula [4]:

$$\mathrm{Abs}_i^{\mathrm{SNV}} = \frac{\mathrm{Abs}_i - \overline{\mathrm{Abs}}}{S} \tag{6}$$

where Abs_i is the original absorbance in the wavelength i; $\overline{\mathrm{Abs}}$ the average absorbance of the spectrum; and S is the standard deviation.

The use of loadings can help deciding which part of the NIR spectra is the most valuable and useful. So, the value of the loadings provides information about the influence of the variables on the final obtained membranes, which will be used to classify them. Loadings show how well a variable is taken into account by the model components, and they can be used to understand how much each variable contributes to the meaningful variation of data. If a variable has a very small loading, whatever the sign of that loading, that variable should not be considered for interpretation, because that variable is badly accounted by the principal components (PC). Fig. 3 shows the loadings of the three first PC for all the membranes. Three different areas are found: (a) 1684–1714 nm; (b) 2274–2444 nm; (c) 2452–2500 nm. Therefore, we selected these three ranges of wavelengths as variables for building the models.

The reason why these wavelengths are the most valuable is because the spectra in the range from 2274 to 2500 (areas b and c) has been formed by a combination of bonds of C–H/C–H and C–H/C–C. The combination is produced when a photon excites simultaneously two modes of vibration. Then the frequency of the combination bands is approximately the sum or the difference of the two fundamental frequencies. In this way, depending to the morphology of the polymer different combinations of bands can be encountered. Besides, the wavelength region between 1684 and 1714 (area a) correspond to the methyl and the aromatic ring bands, respectively, which are two characteristic parts of the polysulfone that may also be affected by the membrane preparation procedure and the final morphology obtained.

3.3. Principal component analysis (PCA)

A classification model for the membrane NIR spectra is presented here, starting with the principal component analysis (PCA) calculation (as a chemometric tool).

Fig. 4 represents the scores for the two first principal components of the membrane NIR spectra, for membranes prepared both by the immersion and the evaporation technique, and for all thicknesses or classes investigated. Scores are estimated using bilinear modeling methods, which imply that the information originally carried by several variables is now concentrated into a few underlying variables. The model calculated has four principal components (PC's) and the two first PC's explained the 96.63% of the original data. The x-axis is the value for the first component and the y-axis is the value for the second component.

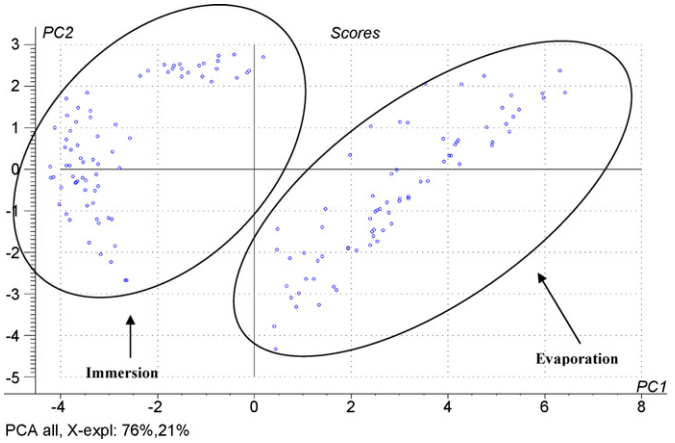

Fig. 4. Scores plot for the 1st and 2nd principal components (PCA) of all the ultrafiltration membranes under study, prepared either by the immersion or the evaporation technique.

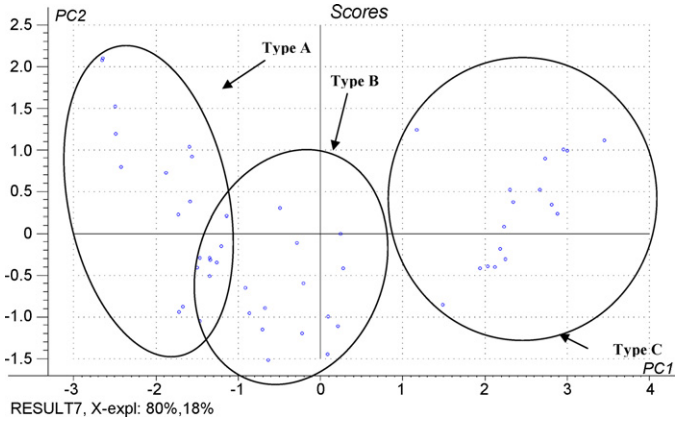

Fig. 5. Scores plot for the 1st and 2nd PCA of the membranes prepared by the immersion technique (type A (26 μm), B (61 μm) and C (95 μm)).

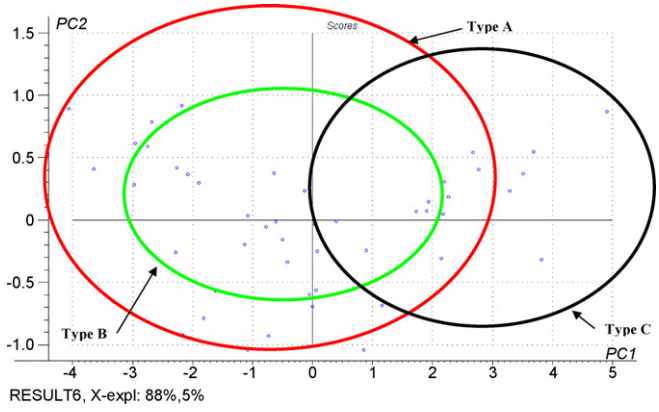

Fig. 6. Scores plot for the 1st and 2nd PCA of the membranes prepared by the evaporation technique (type A (46 μm), B (68 μm) and C (93 μm)).

The scores show the locations of the samples along each model component, and can be used to detect sample patterns, groupings, similarities or differences. It can be observed that with only the first two components it is already possible to distinguish between membranes prepared by the two different techniques.

We also calculated a model for the three different membrane thicknesses obtained by each technique, immersion and evaporation. In case of the immersion technique, the model has three PC's and the 98.59% of the original data is explained by the first two PC's. Class A corresponds to thickness 26 μm, class B to 61 μm, and class C to 95 μm. As seen in Fig. 5, the projection on the first component (*x*-axis) is related with membrane thickness, so types A and C are clearly separated and the B group lies between them, so the three types of membrane are quite well defined. As shown in Table 1, when type B membranes are formed, membranes become more or less thick within a range. For this reason, morphology can be closed to type A or type C membranes. Discriminating between classes A (26 μm membrane thickness) and C (95 μm membrane thickness) is simple as their thicknesses are somewhat different.

The model for the membranes prepared by evaporation explains the 93.36% of the original data for the first two PC's. The scores plot of them presents overlaid points within all three thicknesses, as can be seen from the results shown in Fig. 6. This is probably due to the high similarities in morphology between all these membranes (as previously shown in Fig. 1b).

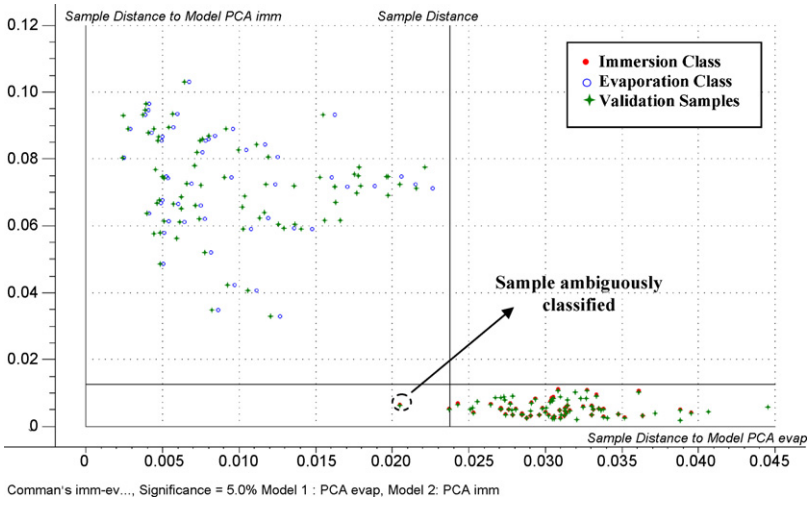

Fig. 7. Cooman's plot for membranes prepared by the immersion and evaporation techniques including the samples for calibration set and validation model.

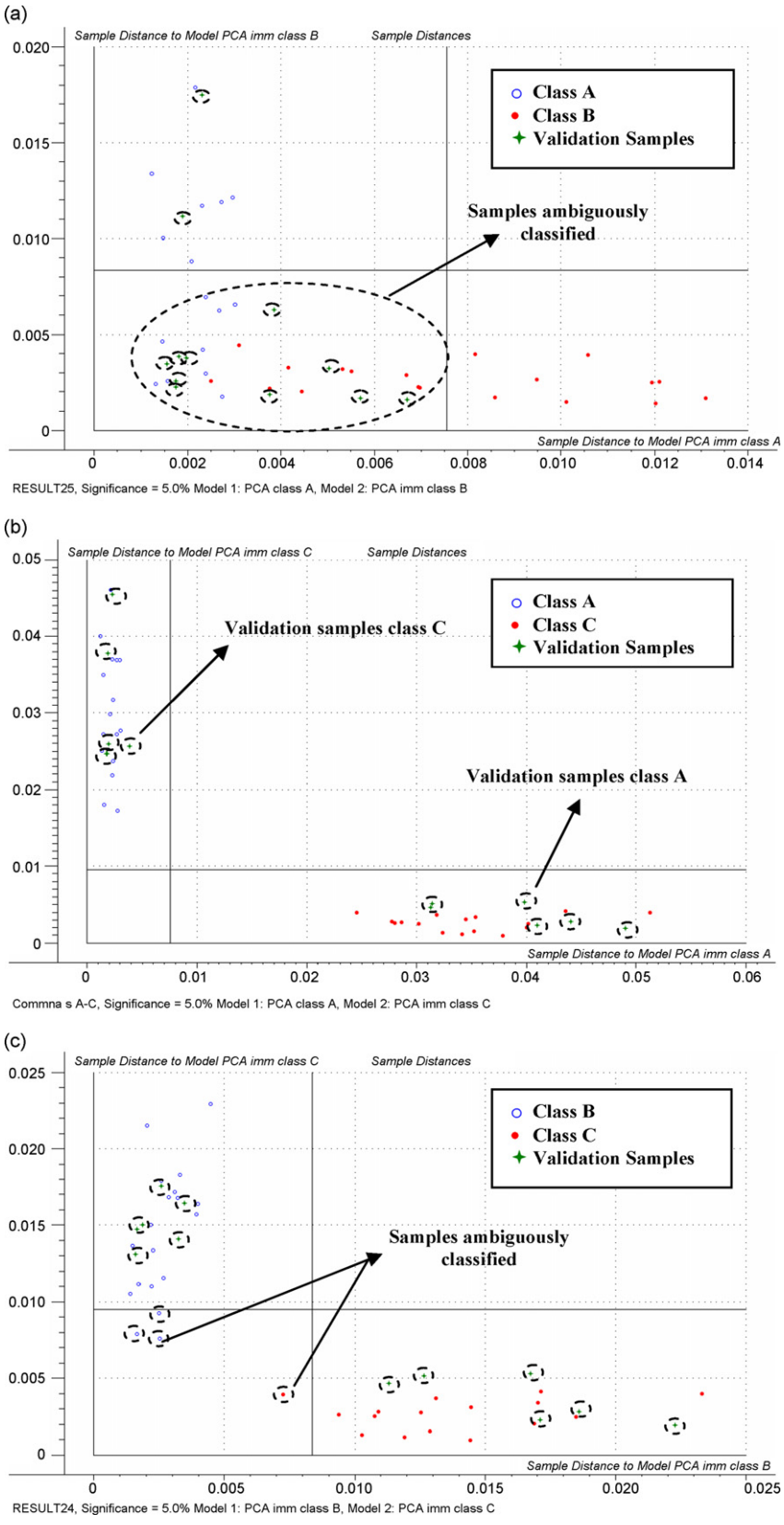

Fig. 8. Cooman's plot for the membranes prepared by the immersion technique: (a) for classes A (26 μm) and B (61 μm); (b) A (95 μm) and C (95 μm); (c) B (61 μm) and C (95 μm), including the samples for calibration set and validation model.

As stated earlier, the characteristics of the absorption bands in NIR spectra depend on both chemical composition and physical properties. In this case, as the chemical composition is exactly the same for all the membranes prepared, either by evaporation or by the immersion techniques, differences in morphology are responsible of differences in NIR spectra. Therefore, the tandem NIR-chemometric tools employed make it possible to distinguish between membranes possessing unlike morphologies.

3.4. Classification of polysulfone ultrafiltration membranes prepared by immersion or evaporation techniques

Here, polysulfone ultrafiltration membranes are classified depending on the preparation technique used. A group of 150 membrane samples was split into the following sets: 100 membrane samples were prepared as the calibration set, 50 of which were prepared by immersion and the other 50 by evaporation; and 50 membranes were prepared as unknown samples to be used as the validation set, 25 of which were obtained by immersion and 25 by evaporation. Besides, each set included membranes of different thicknesses.

As explained in Section 2.6, Cooman's plot allows us to explain the classification of a sample between two classes according to their distance from the class model.

In Fig. 7 samples prepared by immersion and evaporation techniques were compared. Using SIMCA, the class formed by the membranes prepared by the immersion technique may be modeled by three PC's, while the model in the case of the evaporation technique is based on four PC's, accounting for at least 99% of the original information in each case. As seen in figure, only one sample (prepared by immersion technique) is ambiguously classified, as it may belong to both classes. All the 50 validation samples are correctly classified. Therefore, a good prediction model was established for the classification of polysulfone ultrafiltration membranes depending on the preparation technique and procedure used (either by immersion or evaporation techniques).

3.5. Classification of polysulfone ultrafiltration membrane depending on their thickness

Here the objective was to classify membranes of different thicknesses prepared by the same preparation technique (immersion or evaporation). In this case, the classification of the polysulfone ultrafiltration membranes was made in accordance with their thicknesses.

When membranes are prepared by the evaporation technique, their thicknesses cannot be predicted. Comparing membranes and thicknesses by pairs of classes, as was done in the case of immersion, no classes can be defined with the SIMCA model. As has been seen in Fig. 5, when determining the corresponding principal components (PCs), the morphology is too similar within the all membranes and it is not possible to distinguish them by means of their thickness, using the NIR spectra and the aforementioned chemometric model.

In this section, only the results obtained with membranes prepared by immersion technique are presented. The following sets were prepared: 16 membrane samples were prepared as the calibration set, and six samples were prepared to be used as unknowns for the validation set. As before, we have three different thicknesses classified in classes A, B and C. The comparison using Cooman's plot is made two against two.

3.5.1. Classes A and B

In this case, as seen from the corresponding Cooman's plot in Fig. 8a, the morphology of both membranes and their thickness are too close, so it is not possible to either distinguish or validate the model. A large number of the membrane samples of both classes are mixed near to the origin and it is not possible to classify them. So, in the present case, membranes with thicknesses of 26 and 61 μm cannot be classified or distinguished.

3.5.2. Classes A and C

Fig. 8b shows the Cooman's plot for membranes A and C, both prepared by the immersion technique. As can be seen, the classes are separated and the model is perfectly validated (100%). This means that when we have unidentified membranes in storage, it will be possible to classify their thicknesses by only recording their NIR spectra and using the presented chemometric model. In this case, it is possible to distinguish and classify membranes of average thicknesses of 26 and 95 μm, A and C, respectively.

3.5.3. Classes B and C

The corresponding results of the Cooman's plot obtained in this case, comparing classes B and C, are shown in Fig. 8c. When we try to classify them, there are only four samples ambiguously classified in the calibration set and none in the validation set. The model is suitable to be used to predict the thickness of the samples between ca. 61 and 95 μm.

4. Conclusions

Near infrared spectroscopy (NIR) combined with chemometric techniques has come to be a promising technique for characterizing and identifying the polysulfone ultrafiltration membranes prepared here.

From the determination of the principal components (PC), and using SIMCA for classification, a proper model has been determined and validated, which can distinguish between membranes prepared by immersion or evaporation techniques. Unfortunately, the membranes prepared by evaporation are very similar to each other and it is therefore not possible to classify them by thickness using that combination of NIR and chemometric model. Moreover, in the case of membranes prepared using the immersion technique, a model has also been calculated and validated to classify membranes of thicknesses between 84 and 104 μm (identified as class C of 95 μm) in comparison to membranes of between 49 and 72 μm (corresponds to class B and 61 μm), and 24–28 μm (for class A of 26 μm). When increasing the thicknesses of the polysulfone membranes prepared by immersion technique, the macrovoid formation increases affecting to the morphological differences which may be detected by the NIR-chemometric model here proposed.

Thus, NIR and chemometrics offer wide possibilities for classifying membranes with different morphologies or chemical compositions. In the near future, this technique may be implemented to characterize other aspects of membranes, such as fouling in micro-, ultra- and nano-filtration, or to confirm the immobilization of biomolecules/carriers in affinity/facilitated transport membranes.

Acknowledgements

This work was supported by the C.I.C.Y.T. (Ref.: PPQ2002-024201-C02-01, CTQ2005-09430-C05-01 and CTQ2004-02013). Aleix Conesa acknowledges a grant from the *Departament de Química* of the *Universitat Autònoma de Barcelona* (Catalunya, Spain) for the pre-doctoral fellowship. The authors wish to thank the S*ervei de Microscopia Electrònica* of the *Universitat Autònoma de Barcelona UAB* (Catalunya, Spain) for the SEM analysis. Mr. Miguel Castillo is acknowledged for his contribution to the use of the NIR equipment.

References

[1] C. Lubello, R. Gorl, Membrane bio-reactor for textile wastewater treatment plant upgrading, Water Sci. Technol. (2005) 52–91 (4, Upgrading Wastewater Treatment Plants).
[2] M. Soylak, I. Narin, U. Divrikli, S. Saracoglu, L. Elci, M. Dogan, Preconcentration-separation of heavy metal ions in environmental samples by membrane filtration, atomic absorption spectrometry combination, Anal. Lett. 37 (4) (2004) 767.
[3] J. Macanas, D. Muraviev, M. Oleinikova, M. Munoz, Separation of zinc and bismuth by facilitated transport through activated composite membranes, Solvent Extr. Ion Exch. 24 (4) (2006) 565.
[4] M. Resina, J. Macanas, J. de Gyves, M. Munoz, Zn(II), Cd(II) and Cu(II) separation through organic-inorganic hybrid membranes containing di-(2-ethylhexyl) phosphoric acid or di-(2-ethylhexyl) dithiophosphoric acid as a carrier, J. Membr. Sci. 268 (1) (2006) 57.
[5] S. Srisurichan, R. Jiraratananon, A.G. Fane, Mass transfer mechanisms and transport resistances in direct contact membrane distillation process, J. Membr. Sci. 277 (1–2) (2006) 186.
[6] T. Smith Sorensen, Surface Chemistry and Electrochemistry of Membranes Surfactant Science Series, vol.79, Marcel Dekker, 1999.
[7] H.J. Kim, R.K. Tyagi, A.E. Fonda, K. Jonasson, The kinetic study for asymmetric membrane formation via phase-inversion process, J. Appl. Polym. Sci. 62 (1996) 621.
[8] W. Kools, Membrane formation by phase inversion in multicomponent polymer systems. Mechanisms and morphologies, Doctoral Thesis, University of Twente, 1998.
[9] N. Vogrin, Č. Stropnik, V. Musil, M. Brumen, The wet phase separation: effect of cast solution thickness on the appearance of macrovoids in the membrane forming ternary cellulose acetate/acetone/water system, J. Membr. Sci. 207 (2002) 139.
[10] D. Li, T.S. Chung, J. Ren, R. Wang, Thickness depence of macrovoid evoluton in wet phase-inversion asymmetric membranes, Ind. Eng. Chem. Res. 43 (2004) 1553.
[11] A. Conesa, T. Gumí, C. Palet, Membrane thickness and preparation temperature as key parameters for controlling the macrovoid structure of chiral activated membranes (CAM), J. Membr. Sci. 287 (2007) 29.
[12] I.C. Kim, K.H. Lee, Effect of various additives on pore size of polysulfone membrana by phase-inversion precess, J. Appl. Polym. Sci. 89 (2003) 2562.
[13] H.A. Tsai, R.C. Ruaan, D.M. Wang, J.Y. Lai, Effect of temperature and span series surfactant on the structure of polysulfone membranes, J. Appl. Polym. Sci. 86 (2002) 166.
[14] J.Y. Lai, F.C. Lin, C.C. Wang, D.M. Wang, Effect of nonsolvent additives on the porosity and morphology of asymmetric TPX membranes, J. Membr. Sci. 118 (1996) 49.
[15] M. Mulder, Basic Principles of Membrane Technology, 2nd ed., Kluwer Academic Publishers, Dordrecht, 2000.
[16] S. Singh, K.C. Khulbe, T. Matsuura, P. Ramamurthy, Membrane characterization by solute transport and atomic force microscopy, J. Membr. Sci. 142 (1998) 111.
[17] T. Gumí, M. Valiente, K.C. Khulbe, C. Palet, T. Matsuura, Characterization of activated composite membarnes by solote transport, contact angle measurement, AFM and ESR, J. Membr. Sci. 212 (2003) 123.
[18] M. Blanco, J. Pagès, Classification and quantitation of finishing oils by near infrared spectroscopy, Anal. Chim. Acta 463 (2002) 295.
[19] M. Blanco, M.A. Romero, Near-infrared libraries in the pharmaceutical industry: a solution for identity confirmation, Analyst 126 (2001) 2212.
[20] H.M. IESE, A. Bittner, R. Marbach, Clinical chemistry and near infrared spectroscopy: technology for non-invasive glucose monitoring, J. Near Infrared Spectrosc. 6 (1998) 349.
[21] L.A. Cassis, J. Yates, W.C. Symons, R.A. Lodder, Cardiovascular near-infrared imaging, J. Near Infrared Spectrosc. 6 (1998) 21.
[22] U. Hoffman, N. Zandier-Szydlowski, Portability of near infrared spectroscopic calibration for petrochemical parameters, J. Near Infrared Spectrosc. 7 (1999) 33.
[23] D.A. Skoog, J.J. Leary, Principles of Instrumental Analysis, Saunders College, Orlando, Florida, 1992.
[24] M. Blanco, A. Vilar, Polymorphic analysis of a pharmaceutical preparation by NIR spectroscopy, Analyst 125 (2000) 2311.
[25] M. Blanco, D. Valdés, M.S. Bayod, F. Fernández-Marí, I. Llorente, Characteritzation and analysis of polymorphs by near-infrared spectroscopy, Anal. Chim. Acta 502 (2004) 221.
[26] S. Wold, Pattern recognition by means of disjoint principal components models, Pattern Recognit. 8 (1976) 127.
[27] L. Kryger, Interpretation of analytical chemical information by pattern recognition methods—a survey, Talanta Rev. 28 (1981) 871.
[28] K. Pearson, On lines and planes of closest fit to systems of points in space, Philos. Mag. 2 (6) (1901) 559.
[29] S. Wold, K. Esbensen, P. Geladi, Principal component analysis, Chemom. Intell. Lab. Syst. 2 (1987) 37.
[30] M. Otto, Chemometrics. Statistics and Computer Application in Analytical Chemistry, Wiley–VCH, Weinheim, 1999, p. 128.
[31] A. Jos, I. Moreno, A.G. Donzález, G. Repetto, A.M. Cameán, Differentation of sparking wines (cava and champagne) according to their mineral content, Talanta 63 (2004) 377.
[32] G.R. Flåten, B. Grung, O.M. Kvalheim, Quantification of pollution levels by multiway modelling, J. Chemom. 18 (2004) 173.
[33] D. Coomans, I. Broeckaert, M.P. Berbe, A. Tassin, D.L. Massart, S. Wold, Use of a microcomputer for definition of multivariate confidence regions in medical diagnosis on clinical laboratory profiles, Comp. Biomed. Res. 17 (1984) 1.
[34] C. Ventura, M. Papini, Analysis of scattering properties of granular materials, J. Near Infrared Spectrosc. 5 (1997) 123.
[35] R.J. Barnes, M.S. Dhanoa, S.J. Lister, Standard normal variate transformation and de-trending of near-infrared diffuse reflectance spectra, Appl. Spectrosc. 6 (1989) 772.

ANNEX 2

Available online at www.sciencedirect.com
ScienceDirect
Journal of Membrane Science 287 (2007) 29–40
journal of MEMBRANE SCIENCE
www.elsevier.com/locate/memsci

Membrane thickness and preparation temperature as key parameters for controlling the macrovoid structure of chiral activated membranes (CAM)

Aleix Conesa[a], Tània Gumí[b], Cristina Palet[a,*]

[a] *Centre Grup de Tècniques de Separació en Química, Unitat de Química Analítica, Departament de Química, Universitat Autònoma de Barcelona, 08193 Bellaterra, Catalunya, Spain*
[b] *Institut Européen des Membranes, Université Montpellier 2, Place Eugènne Bataillon, CC 047, 34095 Montpellier Cedex 5, France*

Received 30 May 2006; received in revised form 21 September 2006; accepted 1 October 2006
Available online 6 October 2006

Abstract

A macrovoid structure is formed in polysulfone (PSf) polymeric membranes prepared by the immersion technique using *N*-dimethylformamide (DMF)/water as a solvent/non-solvent pair. It is actually important controlling the macrovoid formation process, because macrovoids can cause unwanted mechanical failure during high-pressure applications. In order to control the formation of these structures, the influence of different parameters like membrane thickness, solvent additives (isopropyl myristate, IPM or *N*-hexadecyl-L-hydroxypriline, HHP), temperature of the coagulation bath, and solvent/non-solvent pair has been studied for chiral activated membranes. With the same purpose, corresponding membranes where physically characterized by scanning electron microscopy (SEM) measurements of their cross-section images. Those SEM images have been treated by the software IFME®, which provides the parameters of asymmetry and irregularity of the membranes. The surface of the membranes has been analyzed by atomic force microscopy (AFM) and brightness analysis in order to calculate their roughness. A comparison of the same PSf membranes, but prepared by evaporation precipitation, or by using chloroform/methanol as solvent/non-solvent pair during the immersion precipitation step, has been also checked. That paper helps us to understand and predict which will be the best conditions to prepare the optimum membranes.

Keywords: Polysulfone membranes; Phase inversion; Macrovoids; Thickness; Temperature of coagulation bath

1. Introduction

Nowadays, membrane separation systems are well established, as they offer several advantages over traditional methods, such as low time cost, set-up simplicity and the possibility to be used in continuous mode. One of the most attractive emerging applications of membrane technologies is enantioresolution of racemic mixtures [1].

Various membrane configurations have already been proposed for separating a large number of chiral species, including amino acids and their derivatives, and drugs. Different liquid membrane types, based either on chiral liquids or on solutions of chiral molecules (namely, chiral selectors or carriers), were first proposed to resolve racemic mixtures [1]. Crown ethers, polyaminoacids, cyclodextrines [2] and *N*-hexadecil-L-hydroxyproline [3] are some of the most widely employed chiral molecules. However, liquid membrane processes, when applied for separating enantiomers, have low stability and a short lifetime when tested under industrial separation conditions [4]. Therefore, solid polymeric membranes based mostly on ultrafiltration membranes [5,6] or polymer-imprinting membranes [7] were developed.

In the case of *S*,*R*-propranolol, a β-blocking drug used for treating certain cardiovascular anomalies (with the *S*-enantiomer showing far more blocking activity than the *R*-enantiomer) [8], and various polymeric membrane systems capable of discriminating between both enantiomers have already been proposed [9–11], showing promising results.

However, in order to achieve real progress, the detailed characterization of the chiral polymeric membranes under study

* Corresponding author. Tel.: +34 935813475; fax: +34 935812379.
E-mail address: Cristina.Palet@uab.es (C. Palet).

0376-7388/$ – see front matter © 2006 Elsevier B.V. All rights reserved.
doi:10.1016/j.memsci.2006.10.006

becomes mandatory [12]. This may be elucidated by using different complementary characterization techniques, such as atomic force microscopy (AFM), scanning electron microscopy (SEM), SEM image treatment with IFME® software (Torras, C., registered software no. 02/2003/3395, Spain), and gloss analysis.

AFM allows imaging of non-conducting samples down to nanometer scale. Morphological parameters, including mean roughness and mean pore size, can be obtained from AFM images of membrane surfaces [13].

SEM permits imaging cross-section and surface membrane morphology. Furthermore, treating SEM images with IFME® leads to a relative quantification of certain internal membrane morphological parameters: void dimensions and density, internal asymmetry and overall irregularity [14].

The morphology and the properties of the polymeric membranes have already been studied in detail by different authors. Membrane formation using the phase inversion technique or evaporation technique [12] is often accompanied by the occurrence of large teardrop like voids, namely, macrovoids [15,16]. A wide range of parameters have been checked concerning the formation of macrovoids, such as the membrane preparation technique [10], polymer concentration in the casting solution [17], type of solvent/non-solvent pair [18], membrane thickness [19,20], presence of certain additives [21], and temperature of coagulation bath [22] or the presence of some solvents [23], among others. Knowledge, which allows the macrovoid formation process to be controlled, is very important both to avoid the presence of macrovoids, because they can cause unwanted mechanical failure during high pressure applications, and to improve macrovoid formation when it can be beneficial for efficiently printing the template-functional polymer complex in the case of molecular imprinted membranes (MIP) [24].

In this work, various chiral activated membranes (CAM) investigated previously [25,26] for enantioseparation of propranolol, were prepared and properly characterized. CAMs are polysulfone (PSf) polymeric based membranes prepared either by immersion or evaporation precipitation techniques. Different solvent/non-solvent pairs were also assayed. These were obtained in the presence or not of a solvent modifier such as isopropyl myristate (IPM), and containing the chiral carrier *N*-hexadecyl-L-hydroxyproline (HHP) (previously dissolved in IPM or added directly to the PSf casting solution). Thus, the composition of the membrane casting solution, as well as the procedure to obtain the membranes were properly checked, giving emphasis on membrane thickness and coagulation bath temperature as key parameters for controlling macrovoid structure of chiral activated membranes.

2. Experimental

2.1. Materials

Non-woven fabric (Hollytex 3329) was used as mechanical support for the membranes. The polysulfone (PSf) used in this study was supplied by BASF, Spain under the trade name of Ultrason S3010 incolor. The solvent/non-solvent pairs used were: *N*-dimethylformamide (DMF) (Sigma–Aldrich, Germany)/distilled water, and chloroform (Panreac, Spain)/methanol (Panreac, Spain). *N*-hexadecyl-L-hydroxyproline (HHP) (Sigma–Aldrich, Germany), p.a. grade, was used as the chiral carrier and isopropyl myristate (IPM), p.a. grade, as its solvent.

2.2. Equipment

The cross-section images of the prepared membranes were obtained by a scanning electron microscopy (SEM), Hitachi H-7000 (Hitachi Ltd., Japan, Tokyo). For this purpose the membrane samples were fractured in liquid nitrogen and then coated with gold under vacuum conditions. SEM images were also analyzed by IFME® software for their proper interpretation, as indicated in the introduction.

AFM images were obtained by using a Nano Scope III equipped with a 1553D scanner from Digital Instruments, USA. The tapping mode of AFM in air was used to investigate the membrane surface morphology. Silicone nitride cantilevers were employed.

In order to obtain the membrane brilliance values, a Brightness Analysis of the membrane surfaces was run by using a glossmeter. The measures were obtained by using Table-top Novo-Curve NOFE 0203208 (Rheopoint Inst. Ltd., East Sussex, England).

2.3. Membrane preparation

Four different membrane casting solution were prepared containing: (A) PSf; (B) PSf and IPM; (C) PSf, IPM and HHP; (D) PSf and HHP. For each case, two different solvents, DMF or chloroform, were investigated. Polysulfone and HHP (when added) concentrations were always of 13 and 0.15 wt.%, respectively. In case of IPM and membrane casting solution B, its concentration was varied from 5 to 15 wt.% (for further details, see Section 3.1.3). Membrane casting solutions were rendered homogeneous by continuous agitation of the mixtures during 24 h. The resulting solutions were cast on the surface of a non-woven fabric (polyester of Hollytex® Company) placed over a glass plate. For this purpose, a proper casting knife was used leading to membranes of thickness ranging from 22 to 115 μm.

All the PSf membranes were prepared by phase inversion techniques, either by immersion or by evaporation precipitation. For immersion precipitation the nascent cast membranes were immediately immersed into a water or methanol coagulation bath (depending whether the solvent employed was DMF or chloroform, respectively), together with the glass plate. They were kept immersed for at least 30 min. The bath temperature was varied from 4 to 40 °C. Later, the membranes were rinsed and stored in water until use. In the case of evaporation precipitation, the membrane film solvent (only DMF was checked) was left to evaporate freely at room temperature in an environment of around 40% of relative humidity, and membranes were then dry-stored.

3. Results and discussion

Polysulfone membranes were prepared as indicated using phase inversion techniques, employing two different approaches: immersion and evaporation precipitation. In the first case two different solvent/non-solvent pairs (DMF/water and chloroform/methanol) were assayed, where DMF was the solvent used in the evaporation case. Different membrane casting solutions were also prepared as indicated. Table 1 shows all the membranes that were prepared in this study.

SEM cross-section membrane images are shown in Fig. 1, and correspond to the three different casting solution compositions and the two different membrane preparation procedures here compared: immersion (with two different solvent/non-solvent pairs) and evaporation. Two defined internal morphologies can be seen: (i) asymmetric membranes with macrovoids and (ii) symmetric membranes without macrovoids. Both membrane morphologies are usually encountered for ultrafiltration membranes [12]. The former morphology is found when membranes are prepared by immersion precipitation using DMF/water as the solvent/non-solvent pair [27], as in the present case. This macrovoid structure is a consequence of the fast polymer precipitation rate that arises from a high miscibility between the solvent/non-solvent pair. In previous studies, we can find thermodynamic and kinetic data about the ternary systems DMF/water/PSf [28,29]. As expected, the symmetric membrane morphology is observed when preparing membranes either by DMF evaporation or by immersion precipitation employing chloroform/methanol as the solvent/non-solvent pair. A slow polymer precipitation rate is attained in both cases, due to the low miscibility between the solvent and the non-solvent, or due to a lower phase transition of the DMF when the non-solvent is the water vapour in the air, in the case of evaporation precipitation. Therefore, previously developed chiral activated membranes follow the same morphological behaviour with the casting solution composition and the membrane preparation procedure as polysulfone raw membranes [9].

3.1. Macrovoid characterization by SEM analysis

3.1.1. Influence of membrane thickness on membrane morphology

The three different membrane casting solutions, A, B, and C mentioned above, were considered for preparing membranes using the immersion technique with DMF/water as the solvent/non-solvent pair. SEM cross-section membrane images corresponding to two of these systems are shown in Fig. 2. Membranes of different thicknesses were prepared as indicated, and are shown in the figure for each case. In system A (PSf in DMF), it can be seen that the internal macrovoid dimensions increase as the membrane thickness increases. This phenomenon can be related to the macrovoid formation mechanism during membrane precipitation, described previously by Mulder [12]. This mechanism has been proposed to occur in two consecutive steps: macrovoid initiation and macrovoid growing-up. The macrovoid initiation step takes place in zones of the membrane film where polymer content is poor. These nuclei are mostly present just below the top surface, since a small amount (1–2 wt.%) of water content is enough to phase separate the PS-DMF solutions. So during the initial exposure to the atmosphere, composition of cast film is varied by vapour sorption, especially in the skin regions of the membrane [30]. Finally the macrovoid growing-up step is due to diffusion and displacement of the solvent and non-solvent pair. Therefore, in thin membrane casting solution films, the macrovoid growing-up step is hindered due to the minuscule space between film top surface and bottom.

A very similar mechanism for macrovoid formation was suggested by Smolders et al. [31], and which fits with our findings. They focus on the relative kinetics of the growth of polymer poor droplets and the exchange rate between the solvent and the non-solvent. Due to the large amount of solvent present in the polymer poor droplets, the droplet can be viewed as a coagulation bath with a huge amount of solvent. Therefore, delayed demixing occurs, resulting in a net non-solvent inflow from the surroundings into the droplet, which leads to a macrovoid forming in the final membrane. Finally, the Monte Carlo diffusion model described by Termonia, also proposes that the solvent/non-solvent interaction parameter is the major controlling step in forming macrovoids [32]. They suggest that the non-solvent penetration through skin defects initiates the macrovoids. The faster exchange of solvent for non-solvent through the defects was thought to be responsible for macrovoid growth. On the other hand, when the solvent/non-solvent was chloroform/methanol, whatever the membrane thickness, macrovoids are never encountered due to the slower exchange of chloroform for methanol.

It can also be observed in Fig. 2, that the behaviour of system B (PSf and IPM in DMF) is completely different. Here, the macrovoids located within the membrane structure are finger-like, and their dimensions remain almost constant with respect to the membrane thickness. Strathmann et al. [33] suggested that finger-like macrovoid formation occurs when the non-solvent inflow into the membrane casting film is higher than the solvent outflow. In the present case, we assume that the presence of isopropyl myristate (IPM) in the membrane casting film participates by lowering the initial DMF outflow.

Table 1
List of membrane compositions and precipitation techniques used to prepare the membranes

	Immersion (DMF/water)	Immersion (chloroform/methanol)	Evaporation (DMF)	Evaporation (chloroform)
PSF	√	√	√	√
PSf + IPM	√	√	√	√
PSf + HHP	√	×	√	×
PSf + HHP + IPM	√	√	√	√

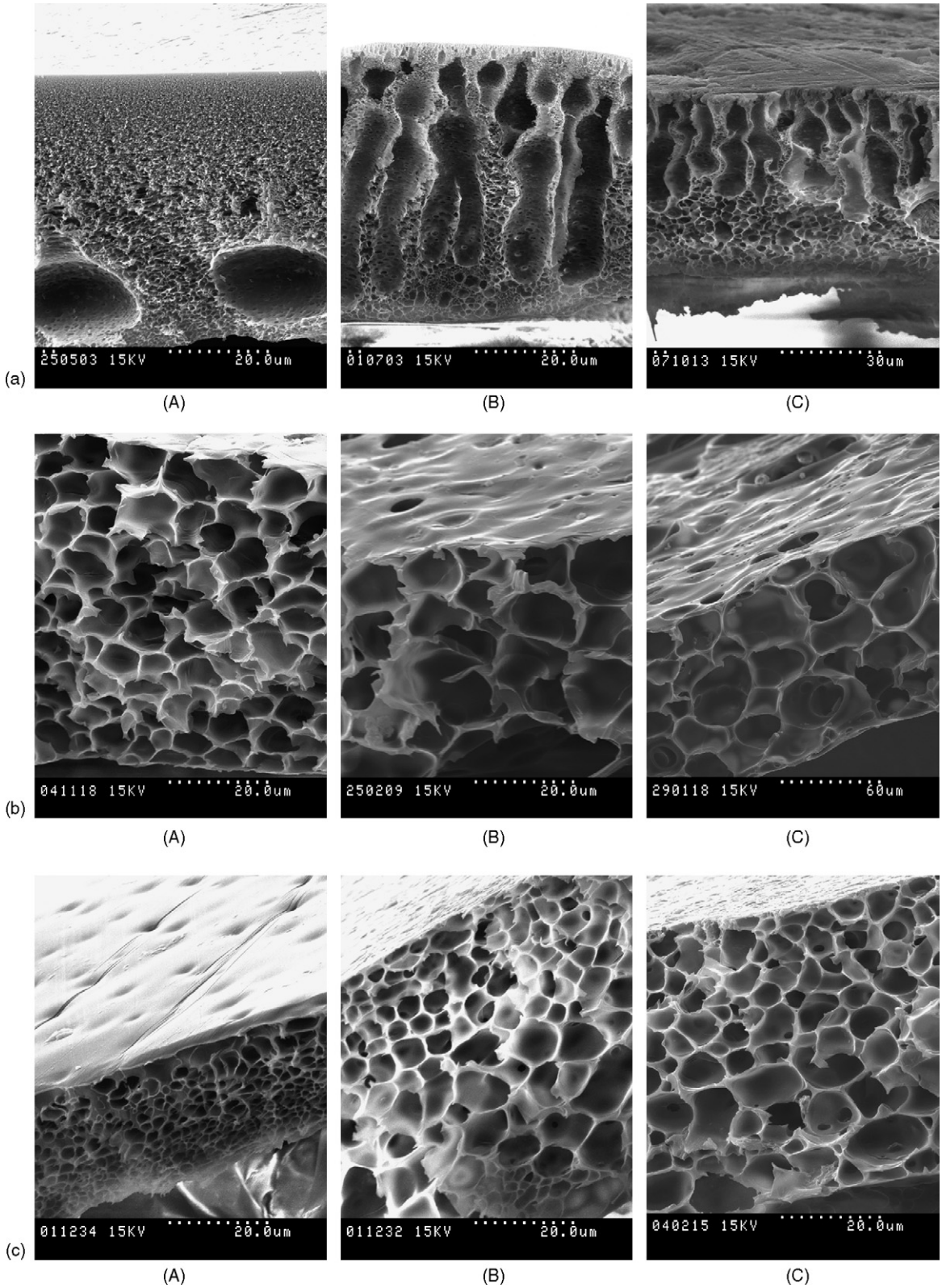

Fig. 1. Scanning electron microscopy (SEM) images of the cross-section morphology of membranes prepared by: (a) immersion (DMF/water); (b) evaporation (DMF as the solvent); (c) immersion (chloroform/methanol). In each case the composition of the casting solution is: (A) PSf, (B) PSf + IPM and (C) PSf + IPM + HHP.

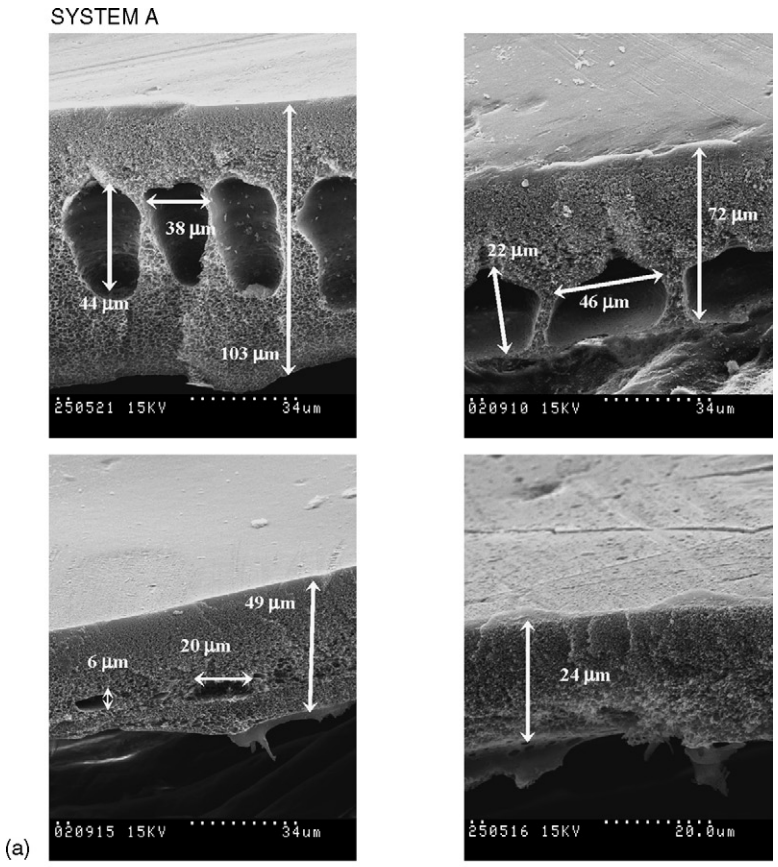

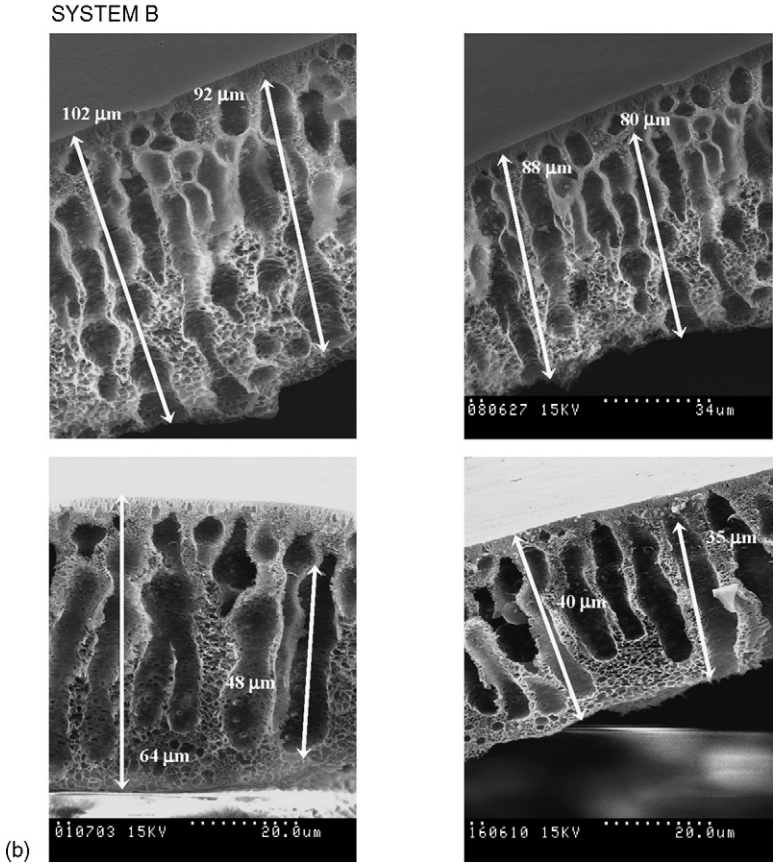

Fig. 2. Effect of membrane thickness on membrane morphology. System composition: PSf 13 wt.%; casting temperature 4 °C; (a) PSf/DMF/water; (b) (PSf + IPM)/DMF/water.

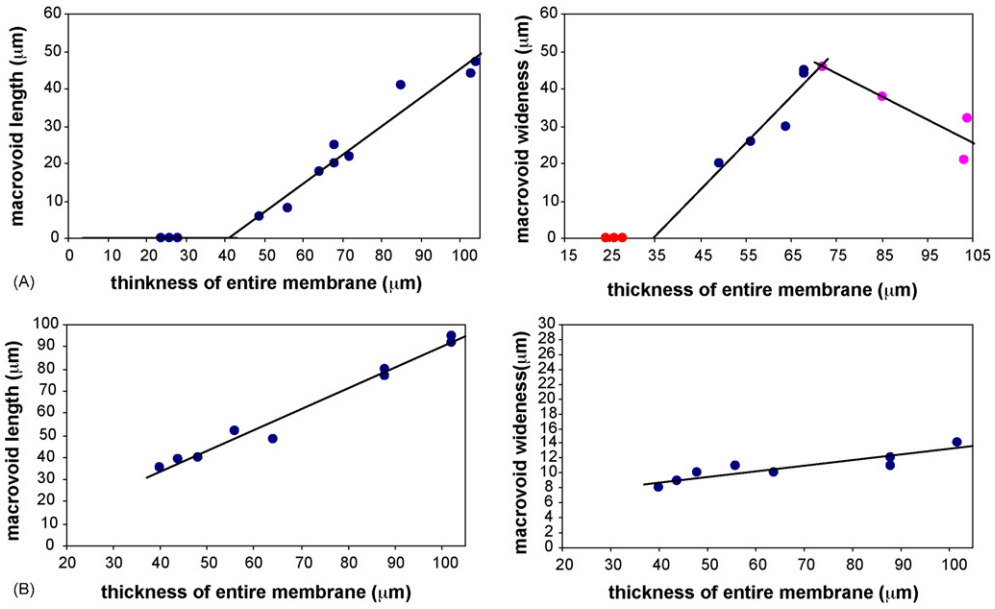

Fig. 3. Effect of membrane thickness on the length and width of macrovoids. System composition: PSf 13 wt.%; casting temperature 4 °C; (A) PSf/DMF/water; (B) (PSf + IPM)/DMF/water.

System C (PSf, IPM and HHP in DMF) is not illustrated because it behaves in the same way as system B.

The measured dimensions (length and width) of macrovoids in membrane systems A and B were plotted versus membrane thickness in Fig. 3. For system A, the macrovoid length increases progressively as membrane thickness increases from ca. 40 μm. However, macrovoid width increases only until a maximum (∼70 μm of membrane thickness) and then decreases. According to the mechanism mentioned above, the initiation step takes place in zones with poor polymer concentration of the membrane film, so near the top. When membranes are thinner than 40 μm, there is not enough space to allow the macrovoid growth-up, while in thicker membranes the non-equilibrium demixing, due to the rapid diffusion of DMF/water pair produces the macrovoid growing-up. In system B, the macrovoid length also increases with membrane thickness, as in system A (from 40 μm). Macrovoid width in this case remains practically unaltered in relation to membrane thickness, which is a typical behaviour of a finger-like macrovoid structure [18].

3.1.2. *Influence of the coagulation bath temperature on membrane morphology*

The same systems A and B where used to assay the influence of the coagulation bath temperature on membrane morphology. Fig. 4 shows the SEM cross-section membrane images of the corresponding membranes. It can be observed that for system A (PSf in DMF) the length and structure of the macrovoids do not vary significantly when the coagulation bath temperature is changed. The same fact was observed previously when using *N*-methylpyrrolidinone (NMP)/water as the solvent/non-solvent pair [34]. It would probably be necessary to increase the temperature further, in comparison with the temperature range studied, in order to decrease the dimensions and number of macrovoids, related to a changes in their miscibility. However, in the case of system B (PSf and IPM in DMF), the studied temperature range is enough to decrease the dimensions and number of macrovoids as the temperature is increased. Fig. 5 shows the variation of macrovoid length with the coagulation bath temperature. In that case, a cast temperature of 40 °C causes almost the disappearance of macrovoids (Fig. 5). This phenomenon is also in agreement with the observations made by Hui-An et al. [34] when they added Span-80 surfactant to their working system. System C (PSf, IPM and HHP in DMF) again behaves in the same way as system B (not illustrated in Fig. 4). The variation of the coagulation bath temperature leads to the modification of both thermodynamic and kinetic properties of the system, which will consequently change the conditions and results of the phase inversion process [35].

3.1.3. *Influence of the IPM concentration in the casting solution on membrane morphology*

Casting solutions with different concentrations of IPM where prepared and used for membrane film precipitation with the immersion technique, using DMF/water as the solvent/non-solvent pair and with the coagulation bath at 4 °C. The corresponding SEM cross-section membrane images are shown in Fig. 6. As can be observed, when the IPM concentration in the membrane casting solution increases, finger-like macrovoids are found. At the lowest IPM amount assayed, the membrane morphology is close to system A (in which there is no IPM), as expected. In Fig. 7, the variation of the membrane thickness/macrovoid length ratio in front of the IPM concentration is shown. It can be observed that when the concentration of IPM is around 10 wt.%, the ratio of membrane thickness/macrovoid is near to 1, which means that the macrovoid has the same length that the membrane thickness, and corresponds to their finger-like structure. Therefore, the concentration of IPM ought to be

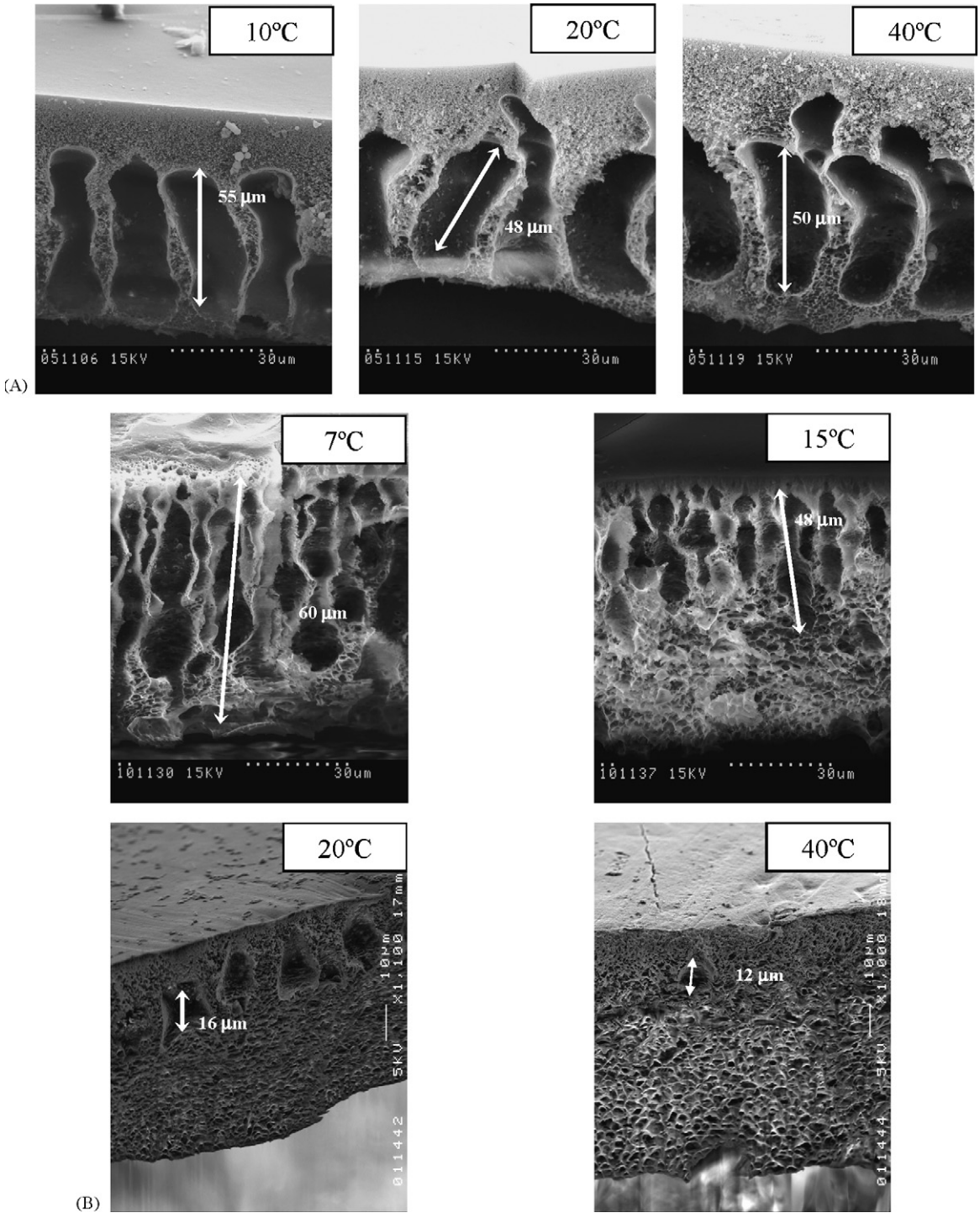

Fig. 4. Effect of bath coagulation temperature on membrane morphology. System composition: PSf 13 wt.%; casting temperature 4 °C; (A) PSf/DMF/water; (B) (PSf + IPM)/DMF/water.

lower than 10 wt.% otherwise the mechanical stability of the membrane might be weak.

3.2. Treating SEM images with IFME®

Table 2 collects all the parameters determined by the IFME® software from SEM images for the most representative membranes prepared. It can be seen that the lowest asymmetry values determined correspond to the membranes obtained with the evaporation technique. In addition, these membranes have the greatest mean void sizes, and consequently the two lowest void densities, as expected [12]. Concerning the membranes obtained with the immersion technique, the presence of macrovoids and their features strongly influ-

Table 2
Membrane characterization parameters obtained by IFME®

Membrane	A	B	C	D	E	F	G
Set	PSF	PSF	PSF	PSF + IPM	PSF + IPM	PSF + IPM + HHP	PSF + IPM + HHP
Technique	Immersion	Immersion	Evaporation	Immersion	Immersion	Immersion	Evaporation
Temperature (°C)	4	4	23	4	20	4	23
Real thickness	24	103	107	80	95	100	102
Density of voids (void, μm^{-2})	0.37	4.0	0.030	0.31	0.060	0.13	0.0012
The average of void (μm)	0.338	1.29	4.52	1.41	2.68	2.23	20.6
The great void (μm)	1.86	18.4	11.9	13.7	10.4	12.6	32.2
The smallest void (μm)	0.100	0.334	2.14	0.250	1.53	1.78	13.6
Standard deviation	0.0264	0.1307	0.6337	0.1948	0.2270	0.6663	1.701
Asymmetry (%)	11	15	9	17	13	27	7
Global irregularity	0.00031	0.0023	0.0010	0.0013	0.00036	0.00095	0.012

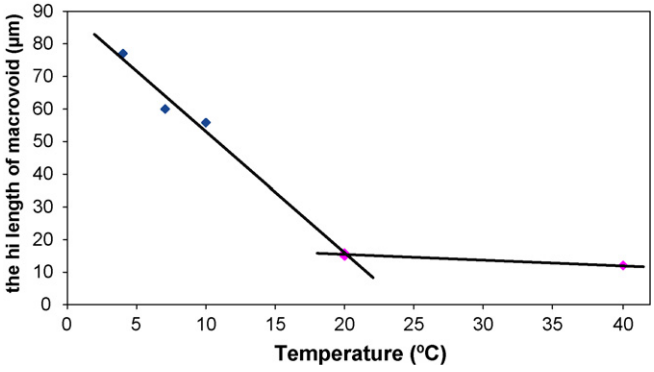

Fig. 5. Effect of bath coagulation temperature on the length of macrovoids. System: PSf 13 wt.%; casting temperature 4 °C; casting solution composition corresponding to system B: (PSf + IPM)/DMF/water.

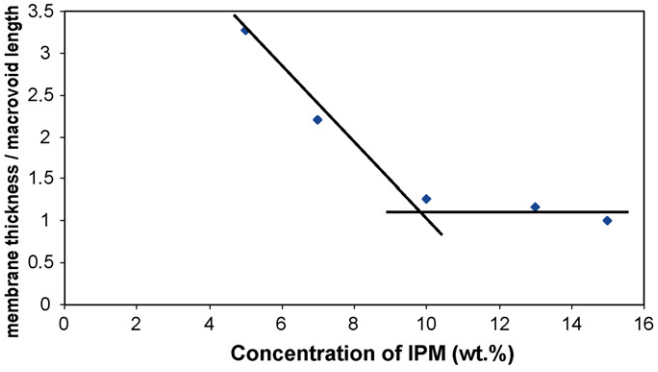

Fig. 7. Effect of IPM concentration on the length of macrovoids. System: PSf 13 wt.%; casting temperature 4 °C; casting solution composition corresponding to system B: (PSf + IPM)/DMF/water.

ence the parameters measured, as seen previously [14]. Therefore, as observed, thickness and bath coagulation temperature influence the asymmetry and the irregularity of these membranes in the way explained above. Thus, the IFME® software allows the relative quantification of membrane morphology features, therefore making it possible to compare different membranes.

3.3. Surface characterization by atomic force microscopy (AFM) analysis

Four membrane systems were analysed by AFM: systems A, B, C and D (PSf and HHP in DMF). In addition, the three membrane preparation techniques mentioned were characterized. AFM images of system C are presented in Fig. 8. Mean roughness (nm) and mean pore size (nm) values of all the

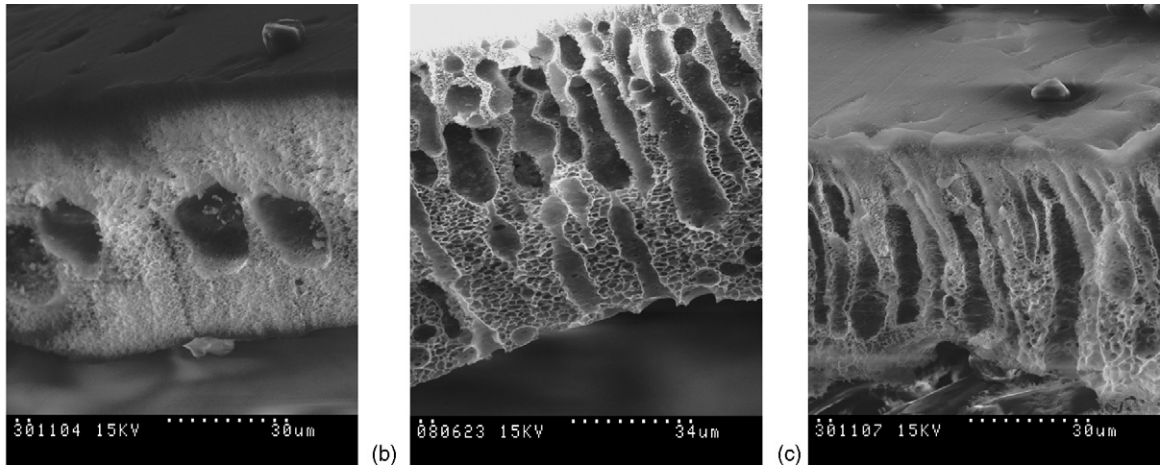

Fig. 6. Effect of IPM concentration on membrane morphology. System: PSf 13 wt.%; casting temperature 4 °C; casting solution composition corresponding to system B: (PSf + IPM)/DMF/water. Concentration of IPM is: (a) 5 wt.%; (b) 13 wt.%; (c) 15 wt.%.

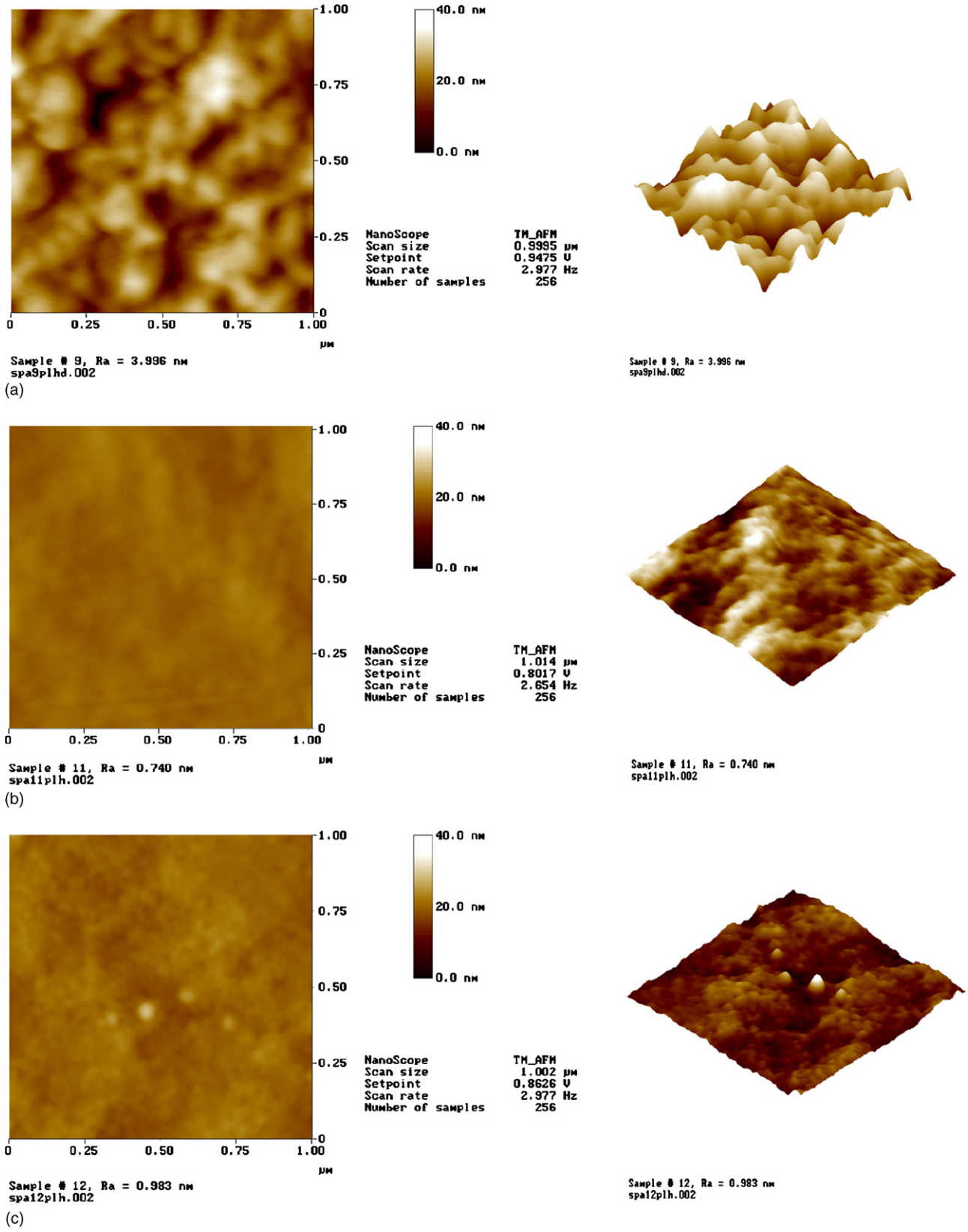

Fig. 8. Atomic force microscopy images of the membrane surface. Casting solution composition corresponding to system D: (PSf + IPM + HHP); casting temperature 4 °C. Preparation technique: (a) immersion (DMF/water); (b) evaporation (DMF/water); (c) immersion (chloroform/methanol).

Table 3
Membrane surface characterization parameters obtained by AFM

System composition	Mean roughness, R_a (nm)	Mean pore size (nm)	Solvent/non-solvent
PSf	3.20	41	DMF/water
PSf + IPM	2.65	34	DMF/water
PSf + IPM + HHP	3.99	44	DMF/water
PSf + HHP	2.57	29	DMF/water
PSf + IPM + HHP	0.74	37	DMF (evap.)
PSf + IPM + HHP	0.98	34	Chloroform/methanol
PSf + IPM + HHP	3.99	44	DMF/water

Table 4
Membrane surface brightness measurements

	PSf (%)	PSf + IPM (%)	PSf + IPM + HHP (%)
Immersion (DMF/water)	74 (±6)	26 (±1)	20 (±2)
Evaporation (DMF solv.)	18 (±1)	10.1 (±0.4)	8.8 (±0.4)

membrane types and preparation techniques are collected in Table 3. No significant differences in terms of mean roughness were found within the four prepared membranes (A, B, C and D). However, clear differences were encountered when comparing membrane preparation methods or the solvent/non-solvent pairs employed (namely, E, F and G experiments in the table) in the case of the immersion precipitation technique. Far lower mean roughness values were found for membranes obtained using the evaporation or the immersion technique, using chloroform/methanol as the solvent/non-solvent pair in the last case. In both cases, dense sponge-like membranes were obtained, as shown in the SEM cross-section images in Fig. 1 [12], which correlates well with their low roughness.

3.4. Membrane characterization by brightness analysis

The three systems A, B and C were used to prepare membranes either using the immersion or evaporation technique as indicated. The brightness of all the obtained membranes was measured. According to Table 4, it can be observed that the membranes prepared using the immersion technique show lower membrane surface brightness when the IPM solvent is incorporated in the membrane casting solution A similar behaviour is observed when membranes are prepared by evaporation, but all values of the membrane surface brightness are lower than the corresponding values of membranes prepared by immersion. There are a clear relationship between the brightness and polymer density: high density cause high data brightness. As, Table 2 shows (IFME results), the density of voids (void, μm^{-2}) of the membrane prepared by immersion technique are ca. 100 times higher than the membranes prepared by evaporation technique. In addition, we can also observe how the presence of IPM in system B, as well as the IPM and HHP in system C (both in immersion and evaporation technique) decrease the density of the polysulfone and therefore the brightness also decrease. The addition of HHP produces a very slight decrease in the density and in consequence in the brightness. Anyway, brightness analyses allow us to indirectly verify the presence of additives, such as IPM and HHP in polysulfone membranes, and also to estimate the phase inversion technique used for their preparation (immersion or evaporation precipitation).

4. Conclusions

We have reported the dependence of macrovoid formation and traits on several membrane parameters: membrane thickness, the membrane preparation method, temperature of the coagulation bath (when using the phase immersion technique), and using casting solution additives. For system A (PSf/DMF/water), we observed that the macrovoid dimensions (length and width) decreased as the membrane thickness decreased until they disappeared completely around 35–40 μm thick. Whereas when isopropyl myristate solvent or carrier *N*-hexadecyl-L-hydroxyproline is added to the casting solution, the macrovoids located within the membranes have a finger-like structure. In this case, only the length of the macrovoids changes with the membrane thickness. The length and structure of macrovoids do not vary significantly when changing the coagulation bath temperature from 4 to 40 °C in system A (PSf in DMF/water). However, in system B (PSf and IPM in DMF/water) and in system C (PSf, IPM and HHP in DMF/water) the presence of macrovoids decreases as coagulation bath temperature increases. Macrovoid formation also depends on the concentration of IPM. High concentrations of IPM in the casting solution produce a larger number of finger-like macrovoid structures.

To obtain reproducible membranes with good resistance under pressure conditions, it is important that macrovoids do not appear. Therefore, when preparing polysulfone membrane we should take into account that one the most important parameter will be the membrane thickness. In this way, the membranes thickness must to be lower than 40 μm, while the temperature of coagulation bath has not influence and could be from 4 until 40 °C.

On the other hand, taking into account our previous works with chiral activated membranes [9,25], the best membrane for

the enantioseparation of the racemic propranolol is the one obtained by using HHP and IPM at 0.15 and 10 wt.% of concentration, respectively, and working with a temperature of the coagulation bath around 20 °C. In that case, we can now suppose that the presence of finger-like macrovoid structures facilitates the transport of propranolol across the membrane, so, the contact between the propranolol and the carrier (which is properly immobilised in the chiral membrane [9,25] is improved).

Certain parameters, such as the mean size of the void, density of voids and roughness, were correlated to the casting solution composition and the corresponding membrane morphology.

The AFM analysis confirms that the presence of IPM and/or HHP do not affect both the surface roughness of the membranes prepared by phase immersion (DMF/water), and their mean pore size. Finally, we introduced the gloss meter analysis to classify the membranes according to both the preparation technique used and the presence of certain additives such as IPM and HHP due to the relationship between the polymer density and brightness.

Acknowledgements

This work was supported by C.I.C.Y.T. (Ref.: PPQ2002-04267-C03-01, PPQ2002-024201-C02-01 and CTQ2005-09430-C05-01). Aleix Conesa acknowledges the grant from la Universitat Autònoma de Barcelona for the pre-doctoral fellowship. The authors want to thank the Servei de Microscopia electrònica of the Universitat Autònoma de Barcelona UAB (Spain) for the SEM analysis. Dr. Khulbe and Dr. Matsuura from the Industrial Membrane Research Institute, IMRI, of the Department of Chemical Engineering of the University of Ottawa (Canada), and Dr. Carlos Muñoz from the Restorative Dentistry Department of the University at Buffalo (USA) are acknowledged for their contribution in the AFM analysis and the brightness data analysis, respectively. Authors want to thank Dr. Carles Torras for his kind help in the IFME analysis.

References

[1] J.T.F. Keurentjes, F.J.M. Voermans, Membrane separations in the production of optically pure compounds, in: A.N. Collins, G.N. Sheldrake, J. Crosby (Eds.), Chirality in Industry. II. Developments in the Commercial Manufacture and Applications of Optically Active Compounds, Wiley, Chichester, 1997.

[2] L.J. Brice, W.H. Pirkle, Enantioselective transport through liquid membranes, in: S. Ahuja (Ed.), Chiral Separations. Applications and Technology, ACS, Washington, 1997, p. 309.

[3] T. Gumi, M. Valiente, C. Palet, Characterization of a supported liquid membrane based system for the enantioseparation of *S*,*R*-propranolol by *N*-hexadecyl-L-hydroxyproline, Sep. Sci. Technol. 39 (2004) 431.

[4] A.J.B. Kemperman, D. Bargeman, Th. Van den Boomgaard, H. Strathmann, Stability of supported liquid membranes: state of the art, Sep. Sci. Technol. 31 (1996) 2733.

[5] T. Masawaki, M. Sasai, S. Tone, Optical resolution of an amino acid by enantioselective ultrafiltration membrane, J. Chem. Eng. Jpn. 25 (1992) 33.

[6] A. Higuchi, H. Yomogita, B.O. Yoon, T. Kojima, M. Hara, S. Maniwa, M. Sayito, Optical resolution of amino acids by ultrafiltration using recognition sites of DNA, J. Membr. Sci. 205 (2002) 203.

[7] M. Yoshikawa, K. Yonetani, Molecularly imprinted polymeric membranes with oligopeptide tweezers for optical resolution, Desalination 149 (2002) 287.

[8] S. Ahuja, Chiral separation and technology. An overview, in: S. Ahuja (Ed.), Chiral Separations. Applications and Technology, ACS, Washington, 1997, p. 1.

[9] T. Gumí, Membranes en la separació enantiomèrica del fàrmac propranolol, Desenvolupament i caracterització, Doctoral Thesis, Universitat Autònoma de Barcelona, 2004.

[10] T. Aoki, M. Ohshima, K. Shinohara, T. Kaneko, E. Oikawa, Enantioselective permeation of racemates through a solid (+)-poly{2-[dimethyl(10-pinalyl)silyl]norbornadiene} membrane, Polymer 38 (1997) 235.

[11] T. Gumí, C. Minguillón, C. Palet, Separation of *S*,*R*-propranolol enantiomers through membranes based on chiral derivatized polysylfone, Polymer 46 (2005) 12306.

[12] M. Mulder, Basic Principles of Membrane Technology, 2nd ed., Kluwer Academic Publishers, Dordrecht, 2000.

[13] T. Gumí, M. Valiente, K.C. Khulbe, C. Palet, T. Matsuura, Characterization of activated composite membranes by solute transport, contact angle measurement, AFM and ESR, J. Membr. Sci. 212 (2003) 123.

[14] C. Torras, R. Garcia-Valls, Quantification of membrane morphology by interpretation of scanning electron microscopy images, J. Membr. Sci. 233 (2004) 119.

[15] L. Zeman, T. Fraser, Formation o fair-cast cellulose acetate membranes. Part I. Study of macrovoid formation, J. Membr. Sci. 84 (1993) 93.

[16] L. Zeman, T. Fraser, Formation o fair-cast cellulose acetate membranes. Part II. Kinetics of demixing and microvoid growth, J. Membr. Sci. 87 (1994) 267.

[17] H.J. Kim, R.K. Tyagi, A.E. Fonda, K. Jonasson, The kinetic study for asymmetric membrane formation via phase-inversion process, J. Appl. Sci. 62 (1996) 621.

[18] W. Kools, Membrane formation by phase inversion in multicomponent polymer systems, Mechanisms and morphologies, Doctoral Thesis, University of Twente, 1998.

[19] N. Vogrin, Č. Stropnik, V. Musil, M. Brumen, The wet phase separation: effect of cast solution thickness on the appearance of macrovoids in the membrane forming ternary cellulose acetate/acetone/water system, J. Membr. Sci. 207 (2002) 139.

[20] L. Dongfei, C. Tai-Shung, R. Jizhong, W. Rong, Thickness depence of macrovoid evolution in wet phase-inversion asymmetric membranes, Ind. Eng. Res. 43 (2004) 1553.

[21] K. In-Chul, L. Kew-Ho, Effect of various additives on pore size of polysulfone membrane by phase-inversion process, J. Appl. Polym. Sci. 89 (2003) 2562.

[22] T. Hui-An, R. Ruoh-Chyu, W. Da-Ming, L. Juin-Yih, Effect of temperature and span series surfactant on the structure of polysulfone membranes, J. Appl. Polym. Sci. 86 (2002) 166.

[23] L. Juin-Yih, L. Fung-Ching, W. Cheng-Chuan, W. Da-Ming, Effect of nonsolvent additives on the porosity and morphology of asymmetric TPX membranes, J. Membr. Sci. 118 (1996) 49.

[24] M. Ramamoorthy, M. Ulbricht, Molecular imprinting of cellulose acetate-sulfonated polysulfone blend membranes for rhodamine B by phase inversion technique, J. Membr. Sci. 217 (2003) 207.

[25] T. Gumi, M. Valiente, C. Palet, Elucidation of *S*,*R*-propranolol transport rate and enantioselectivity through chiral activated membranes, J. Membr. Sci. 256 (2004) 150.

[26] T. Gumí, Q. Ferreira, R.M.C. Viegas, J.G. Crespo, I.M. Coelhoso, C. Palet, Enantioselective separation of propranolol by chiral activated membranes, Sep. Sci. Technol. 40 (4) (2005) 773.

[27] P. van de Witte, P.J. Dijkstra, J.W.A. van den Berg, J. Feijen, Phase separation processes in polymer solutions in relation to membrane formation, J. Membr. Sci. 117 (1996) 1.

[28] M.J. Han, D.J. Bhattacharyya, Changes in morphology and transport characteristics of polysulfone membranes prepared by different demixing conditions, J. Membr. Sci. 98 (1995) 191.

[29] C. Barth, M.C. Gonçalves, A.T.N. Pires, J. Roeder, B.A. Wolf, Asymmetric polysulfone and polyethersulfone membranes: effects of thermodynamic conditions during formation on their performance, J. Membr. Sci. 169 (2000) 287.

[30] M.J. Han, P.M. Bummer, M. Jay, Phase transitions of polysulfone solution during coagulation, Polymer 36 (24) (1995) 4711.

[31] C.A. Smolders, A.J. Reuvers, R.M. Boom, I.M. Wienk, Microstructure in phase inversion membranas. Part I. Forming of macrovoids, J. Membr. Sci. 73 (1992) 259.
[32] Y. Termonia, Fundamentals of polymer coagulation, J. Polym. Sci., Part B: Polym. Phys. 33 (1995) 279.
[33] H. Strathmann, K. Kock, P. Amar, R.W. Baker, The formation mechanism of asymmetric membranes, Desalination 16 (1975) 179.
[34] T. Hui-An, R. Ruoh-Chyu, W. Da-Ming, L. Juin-Yih, Effect of temperature and span series surfactant of the structure of polysulfone membranes, J. Appl. Polym. Sci. 86 (2002) 166.
[35] Q. Zheng, P. Wang, Y. Yang, Rheological and thermodynamic variation in polysulfone solution by PEG introduction and its effect on kinetics of membrane formation via phase-inversion process, J. Membr. Sci. 279 (2006) 230.

ANNEX 3

PREPARATION, CHARACTERIZATION AND APPLICATION OF MOLECULARLY IMPRINTED MEMBRANES (MIM) FOR THE SEPARATION OF DL-SELENOMETHIONINE

Aleix Conesa, [1] Míriam Pérez-Tujillo,[2] Tània Gumí [3] and Cristina Palet [1,*]

[1] *Centre Grup de Tècniques de Separació en Química, Unitat de Química Analítica, Departament de Química, Universitat Autònoma de Barcelona, 08193-Bellaterra, Catalunya, Spain.*

[2] *Servei de Ressonància Magnètica Nuclear, Universitat Autònoma de Barcelona.*

[3] *Departament d'Enginyeria Química, ETSEQ, Universitat Rovira i Virgili, Av. Països Catalans 26, 43007-Tarragona, Catalunya, Spain.*

* Corresponding author. E-mail: Cristina.Palet@uab.es, Fax: +34935812379, Tel: +34935813475.

Abstract

Selenium is an essential element for the human an animal health. Selenomethionine and particularly L-selenomethionine is the majority specie of selenium that we find in the natural foods. In consequence, the assimilation with the nutrition to create stock of selenium in the body is less effective with selenite than with selenomethionine. [1] Besides, L-selenomethionine presents antioxidant effect and it is better retained in the corporal tissues. On account that the L-selenomethionine can not be synthesized by animals and humans the way to administrate the L-selenomethionine in the diet is by biofortification of yeast or wheat, or by the asymmetric synthesis route. An alternative may be the separation of the racemic by membrane technology. Here we present the possibility to separate the chiral mixture of DL-selenomethionine by Molecularly Imprinted Membranes (MIM) separating. Four types of MIM were prepared over an hydophobic polyvinylidene fluoride (PVDF-phob) support using 4-vinylpiridine

(4VPY), methacrylic acid (MAA), acrylamide (AAM) or N,N-dimethyl-2-aminoethylmethacrylate (DMAEM) co-polymerized with the cross-linker glycol dimethacrylate (EDMA). Polymerization was performed in methanol solvent, employing benzoin ethyl ether (BEE) as initiator, and following the M. Ulbricht et. al. process. The separation was carried out in a dialysis membrane cell at different pH phases conveniently buffered.

Different techniques such as Scanning Electron Microscopy (SEM), Attenuated Total Reflection/Fourier Transform Infrared (ATR/FTIR) and solid-state ^{13}C Cross-Polarization Magic Angle Spinning (CP/MAS) Nuclear Magnetic Resonance (NMR) were used to ensure that the co-polymer deposition on the PVDF-phob supported. Besides, other types of characterization such as degree of modification or water flux were calculated.

The best chiral separation between the racemic DL-selenomethionine was obtained in case of the imprinted membrane synthesised with the monomer DMAEM. The optimum conditions was at pH 6 of feed and stripping phases and the separation factor obtained was 1,75.

Keywords: Molecularly Imprinted Membranes (MIM), D L-Selenomethionine, Characterization, Chiral separation.

1. Introduction

Many biochemical processes are based on the molecular recognition phenomenon. The interactions within the natural biomolecules such as enzymes, antibodies, nucleic acid, cellular receptor, etc., are the key factor of the molecular recognition mechanism such as enzymes, antibodies, nucleic acid, cellular receptor, etc. [2] In the last years many approaches have been developed to obtain artificial systems able to mimic the biological

molecular recognition. Molecularly imprinted polymers are gaining importance during the recent years because of their potential of recognition and the simplicity of their preparation. The molecular imprinting procedure is generally based on the linkage of suitable monomers, containing functional groups, to template molecules by covalent or non-covalent interactions. Subsequent copolymeritzation of the resulting template-monomer assembly with an excess of cross-linking agent, in the presence of a porogenic solvent, produces rigid macroporus polymers. Final removal of the template molecules leaves cavities in the polymer whose size, shape and three-dimensional arrangement of binding sites are determined by the structure of the template molecules [3].

The origin of molecular imprinting was introduced by M.V.Polyakov in 1931, [4] who performed a series of investigations on silica for use in chromatography. The technique was further developed and in 1972 molecular imprinting in synthetic organic polymers was reported for the first time by the groups of I.M. Klotz [5] and G. Wulff [6]. They developed an imprinted polymer structure using covalent interactions. In 1994, the group of K. Mosbach [7] established a new technique to obtain molecularly imprinted polymers (MIPs) by a non covalent route (based on electrostatic or hydrogen bonding). This last method became attractive since the corresponding MIPs can be easily prepared. Therefore they have been widely used. Most of the molecularly imprinted polymers are synthesized by free radical copolymertization of functional vinyl monomers with an excess of cross-linking divinyl monomers in solvent medium. In addition, templates are added prior to polymerization in order to form the imprinted sites. In 1990, S.A. Piletsky started the investigation of the transport through imprinted membrane. From this moment, various MIM applications have been published in the literature and are collected in the reviews of S.A. Piletsk et.al. [8] and M. Ulbricht [9]. Although the contributions have notoriously increased the MIM are still emerging.

Nowadays, two techniques are established to prepare MIM: phase inversion in the presence of template molecules [10, 11, 12, 13, 14, 15] and photo-grafting polymerization. [16, 17, 18, 19] Both of them are based on formation of footprints on the pore surface and/or in the bulk polymer.

We have focused on the application of molecularly imprinted polymers, for the preparation of membranes capable to enantioseparate D L-selenomethionine. Selenium is an essential element for the human an animal health, [20] although high levels (over 1ppm) become toxic. In 1973, selenium was identified as a component of the enzyme glutathione peroxidase (GPX) which develops an important role in human body protecting the oxidation's cells. [21] In addition, selenium has also anti-viral and anti-cancer effects.

The characterization of the MIM is a necessary and important rule to know the chemical and structural composition of the polymer as well as the pore system, surface areas, texture, thermostability. [3] For this purpose several techniques are used in Molecularly Imprinted Polymer (MIP) and also applied in the MIM's characterization. Attenuated Total Reflection/Fourier Transform InfraRed (ATR/FTIR) is a useful technique for insoluble polymer that provides chemical information. [22, 23] Another possibility is the use of solid-state CP/MAS NMR. Until now, few publications have reported about the use of this technique in molecularly imprinted polymer, [24, 25, 26, 27] but none concerning MIMs. The main interest of this technique is the possibility to estimate of the relative amounts of different types of carbon atoms have been made for insoluble polymers. The morphological structure and pores systems are usually evaluated by microscopy techniques such as Scanning Electron Microscopy (SEM) or Atomic Force Microscopy (AFM). Other important factor in molecularly imprinted is to verify the template addition in the polymer. The current procedure to extract the template in the

published articles is extracting the membrane at several hours with some solvent or mixture solvents until the UV absorbance is continue and less than 0.005 at 258 nm. In our case we used this method using water and methanol using inductively coupled plasma mass spectroscopy (ICP-MS) to ensure the proper removal of the template, before using the MIMs, In addition, SEM with X-ray microanalysis [28, 29] became very useful tool in case of the presence of inorganic elements.

L-selenomethionine can not be synthesized by animals and humans. Up to now, the way to produce L-selenomethionine is by biofortification of yeast or wheat, [30] and by the synthetic route. [31, 32] Both methods are suitable for nutritional Se-supplementation. [33] In this work, we have developed molecularly imprinted membranes for the separation of the enantiomers DL-selenomethionine. These MIMs represent an alternative technique to obtain L-selenomethionine.

2. Experimental

2.1. Materials

Hydrophobic polyvinylidene fluoride (PVDF-phob, Durapore) microfiltration membranes, with a nominal pore size of 0.22 μm, a thickness of 125 μm and a diameter of 4,7 cm were supplied from Millipore (USA) and used in this work as porous supports for the molecularly imprinted membranes.

Benzoin ethyl ether (BEE), ethylene glycol dimethacrylate (EDMA), 4-vinylpiridine (4VPY), methacrylic acid (MAA), acrylamide (AAM), N,N-dimethyl-2-aminoethylmethacrylate (DMAEM) and methanol (MeOH) were obtained from Sigma-Aldrich (Germany). The racemic DL-selenomethionine and also L-selenomethionine were purchased from Acros Organics (USA). All the products were of analytical grade. MiliQ-water was used when needed.

2.2. Synthesis of molecularly imprinted membranes (MIM)

In order to create radicals and start the grafting copolymerization in the monomer mixture, benzoin ethyl ether (BEE) was used as a α-scission photoinitiatior. [34] The main advantage of this photoinitiator is the possibility of synthesize the molecularly imprinted polymer on any kind of polymer support because no chemical reaction with the support material is involved. On the contrary, with other photochemical initiators like benzophenone, the reaction takes place due to the hydrogen-extraction or removal from the support polymer by the photo-exited benzophenone. [17, 35] Moreover, higher initiation rates close to the surface of the supported could be expected if the surface is coated with the BEE photoinitiator in comparison with the thermoinitiator 2,2'-azobisisobutyronitrile (AIBN), which requires 24 h of UV irradiation. [16, 36] Hence, BEE initiator appeared to be the most appropriate, and according to V. Kochkodan et al. studies, a soaking time of 10 minutes in a 0,25 M methanol solution of BEE was here selected/established. Afterwards, the solvent was evaporated and the supports were immersed again in 10 ml methanol solution with a concentration of 100 mM of (one single) monomer (4VPY, MAA, AAM or DMAEM), 300 mM of EDMA (as the cross-linker) and 5 mM of the L-selenomethionine (as the template). The samples were UV irradiated at wavelength of 350 nm, at various exposure times. After polymerization, membranes were treated with methanol and water solution in order to properly remove the template. The efficiency of this procedure was checked following the absorbance of the extracting solution at 258 nm. The extraction process was considered complete when absorbance was under 0.005. Also, in order to better quantify the amount of the L-selenomethionine removed from MIMs, the extracting solution was analysed by inductively coupled plasma mass spectroscopy (ICP-MS).

2.3. Filtration experiments

To ensure that the chemical modification of the PVDF-phob support do not block or damage it, the flux through the prepared membrane was calculated after the polymerization. A dead end module cell of 35 mm diameter and with a volume of 80 cm^3 was used for measuring water flux at different operating pressures.

Evaluation of membrane enatioseparation ability of such MIMs took place in a methacrylate dialysis cell having two compartments (capacity of 200 ml for both) connected through a circular window where the membrane was placed. Feed and stripping reservoirs were filled with corresponding aqueous solutions, and 500 ppb of DL-selenomethionine was added in feed solution. Diverse feed and stripping aqueous phases at different pH values (conveniently buffered) were here investigated.

Independently of the composition of the membrane, the two main characteristic factors are its flux and its selectivity. So, the analyte transport rate was calculated in terms of flux (J) defined as the decrease of analyte concentration in the feed phase matter with time, t, and for unit area, *A*:

$$J = -\frac{V \cdot dC_f}{A \cdot dt} \qquad \text{equation 1}$$

where V and C_f are the volume and the concentration of feed solution, respectively.

The parameter used to determine the selectivity of the membrane, in terms of the separation between the DL-selenomethionine enantiomers, was the separation factor α:

$$\alpha = \frac{\left(\frac{Cs_{t,D}}{Cs_{t,L}}\right)}{\left(\frac{Cf_{0,D}}{Cf_{0,L}}\right)} \qquad \text{equation 2}$$

where $Cs_{t,D}$ and $Cs_{t,L}$ are the concentration of enantiomers D- and L-, respectively, in the stripping solution at time t, and $Cf_{0,D}$ and $Cf_{o,L}$ are their initial concentrations in the feed solution.

When the transport though the membrane is governed by a facilitated transport mechanism or some unknown transport that can modify the driving force, other useful form to evaluate the transport rate of the analytes across the membrane is to calculate its capacity of re-extraction (R) as follows:

$$R = \left(\frac{Cs_{t,i}}{Cf_{0,i}}\right) \cdot 100 \qquad \text{equation 3}$$

where $Cs_{t,i}$ is the concentration of the analyte i in the stripping solution at time t and $Cf_{0,i}$ is the initial concentration of the same analyte in the feed solution. Thus, the re-extraction is the analytes extraction capacity from the membrane to the stripping phase.

The variation of the amount of each enantiomer in both feed and stripping solution was determined periodically from withdrawn samples by a high pressure liquid chromatography with an ultra violate detector (HPLC-UV). An HPLC Thermo (USA) equipped with a n autosampler AS3000, gradient pumps P 4000 and UV detector UV6000LP, with measurement facility at 192 -800 nm , equipped with ChromQuest Software was employed. The separation was performed on a Chirobiotic T column (25064.6 mm id) using an isocratic flux of 1 ml/min with a mobile phase of water with

2% of methanol and detection at 218 nm, method previously reported by A. Sanz Medel et. al. [37]

2.4. Membrane characterization

Membrane images were obtained by a Scanning Electron Microscopy (SEM), Hitachi H-7000 (Hitachi LTD. Japan, Tokyo). For this purpose, membrane samples were coated with gold and transferred into the microscope. In the case of the cross-section images, firstly, the membrane samples were submerged in ethanol, then frozen in liquid nitrogen and fractured.

Attenuated Total Reflection/Fourier Transform InfraRed (ATR/FTIR) spectra of the polymeric support and MIMs were determined using a model FTIR spectrometer obtaining transmittance spectra in front of wave number (cm^{-1}).

All solid-state ^{13}C Cross-Polarization Magic Angle Spinning (CP/MAS) Nuclear Magnetic Resonance (NMR) experiments were performed on a Bruker AVANCE-400 (Bruker Biospin. Germany) spectrometer equipped with a double tuned 4mm probe, operating at a resonance frequencie of 100.62 MHz for ^{13}C nuclei. The Magic Angle (MA) was adjusted using KBr (purchased from Sigma-Aldrich, Germany). The Hartmann-Hahn condition for 1H→13C CP experiments was determined using the ^{13}C signal of adamantane (purchased from Sigma-Aldrich, Germany). ^{13}C CP/MAS NMR spectra were recorded with a CP contact time of 1 ms, a repetition time of 4 s and a spinning rate of 12 kHz. The ^{13}C chemical shifts were externally referenced to tetramethylsilane (TMS). Each sample was packed into a 4 mm o.d. zirconium rotor and sealed with a Kel-F endcap. The characterisation by CP/MAS NMR was carried out for (a) the PVDF-phob membrane support (b) the molecularly imprinted polymer synthesized without the presence of the PVDF-phob support and (c) the molecularly

imprinted polymer synthesized on the PVDF-phob support. In cases (a) and (c) the sample consisted of small square pieces of membrane (ca. 3 x 3 mm) inserted into the rotor and completely filled with KBr, whereas in (b) the solid polymer (20 mg) is mixed with KBr and inserted homogenously into the rotor. In the former cases (a and c), the detection experiment was repeated considering different orientations of the membrane inside of the rotor and reproducible results were obtained.

The degree of modification (DM) was used as a parameter to estimate/calculate the amount of molecularly imprinted polymer deposited on the PVDF-phob support. It was calculated from the difference in weight between the final MIM and the initial support. The reproducibility of DM values was less than 15%, similar than previously works. [38]

3. Results and Discussion

3.1. Preparation of Molecularly Imprinted Membranes (MIM)

In order to assess the correct preparation of MIMs, various parameters were investigated, i.e. the degree of modification (DM), which depends on the time of polymerization under UV radiation, and the concentration of initiator, as well as the total or global membrane composition. Figure 1 shows the degree of modification (DM) of the four monomers checked: 4-vinylpiridine (4VPY), methacrylic acid (MAA), acrylamide (AAM) and N,N-dimethyl-2-aminoethylmethacrylate (DMAEM) for the different radiation time investigated. The concentration of initiator was constant and equal for all the cases (see section 2.2). As it can be observed, during the first hour of exposition of UV radiation, especially in the first 10 minutes, the DM varies remarkably following an exponential curve. Similar behaviour was obtained in the literature [34, 39]. Nevertheless, the polymerization was studied for 24 hours and the highest DM

was obtained ca. after 3 h of polymerization for all monomers. After this time a plateau appears and no variation of the DM with the time was observed in all cases. In the case of AAM, no relevant data were found due to experimental failures. The different DM for each monomer can be related to kinetic and structural aspects related with the copolymerization procedure between the monomer and the cross-linker, even this is not the objective of this work. [40, 41] It has to take into account that even though all the polymerizations were between monovinyl monomer and divinyl monomer (cross-linker) the different functional groups of each monomer can effect the polymerization reaction, particularly when the liner chains of the monomer are bonded with the cross-linker.

The structural variation of the MIMs was checked by SEM and AFM. Scanning electron microscopy (SEM) was used to analyse the surface and the cross-section of MIMs, and atomic force microscopy (AFM) was employed to evaluate their mean pore diameter and their surface roughness.

SEM surface images for the membranes prepared with the four monomers: 4-vinylpiridine (4VPY), methacrylic acid (MAA), acrylamide (AAM) and N,N-dimethyl-2-aminoethylmethacrylate (DMAEM) co-polymerized with ethylene glycol dimethacrylate (EDMA) and the membrane of PVDF-phob are showed in figure 2. Depending on the type of monomer used the top layer was more or less thick. As can be seen, the PVDF-phob support (figure 2a) presents a porous structure with a nominal pore size of 0.22 μm. After the polymerization the size of the pores decreased as a result of the deposition of the molecularly imprinted polymers on the support surface. In case of 4VPY (figure 2b), the co-polymer formed was composed by small spheres of 1 μm diameter and practically no pores are found. [42] For the MAA case the structure of PVDF-phob remains almost the same as the support surface, so the polymerisation hardly occurs. Finally, when AAM and DMAEM were employed (figure 2d and 2e), a

polymer layer over the polymeric support is encountered. In both cases, the pores of PVDF-phob (the support) are totally covered. On the other hand, the corresponding cross-section images collected in figure 3 show that DMAEM form a narrow layer of co-polymer with a 3,5 μm of width over the PVDF-phob support. The other monomers do not present any observable change in cross-section images and we can consider that the polymer synthesised was penetrated slightly into the support with any visible changes.

3.2. Chiral separation

The separation factors of DL-selenomethionine with the blank support and with different molecularly imprinted membranes, which were obtained by polimerization of the previously mentioned monomers (i.e.: 4VPY, MAA, AAM, DMAEM), are listed in Table 1. The pH of feed and stripping solutions was kept at 8 in all the experiments. When employing acrylamide (AAM) as monomer, no separation of the enantiomers was found. In the case of using the monomers methacrylic acid (MAA) or vinylpiridine (4VPY) certain similar enantioseparation factors were detected, about 1, 20 in both cases. Finally, the use of N,N-dimethyl-2-aminoethylmethacrylate (DMAEM) leaded to the best separation factor encountered, 1, 37. Similar α values has been found by *Sueyoshi et al.* [43,44] and M. Yoshikawa et al. [45] for aminoacids separation although in that studies they used molecularly impreinted membranes prepared by polysulfone, cellulose acetate and peptides derivates. The no separation of DL-selenomethionine when using acrylamide as a monomer for the MIM, may be attributed with the uncharged functional group of the AAM. The corresponding amide group can not exchange its proton between the selenomethionine, and the hydrogen bonds between both are not strong enough for the chiral recognition. [46]. For the other cases, and

comparing with the literature, the monomer DMAEM was previously used with the objective to detect species with alcohol groups [47], and some polar templates such as nucleotides or amino acids [48, 49, 50]. On the order hand, 4VPY was used with templates with carboxylic acid groups, [51], alcohols [52] aminoacids [53] among other. And MAA with templates that are able to establish hydrogen bonds and/or accepting protons. [54, 55, 56] Thus, we expected that the three monomers would be useful for the chiral separation, because our template (L-selenomethionine) is an amino acid with a carboxylic group, which is able to exchange a proton or to establish some hydrogen bonds with the corresponding monomer. In this sense, our results for MAA, 4VPY and DMAEM with a separation factor >1 were expected, (even we would need more detailed investigation to be able to explain the higher value obtained for DMAEM).

Concerning these results, further and detailed characterization of both the enantioseparation process (aqueous phases, pH, cross-linking agent…), and the polymerisation method (polymerisation confirmation), was carried out only for MIM obtained from the monomer DMAEM.

3.3 DMAEM-MIM characterization.

To assure the proper preparation of the MIM, different characterization techniques were employed, such as ATR/FTIR, ^{13}C CP/MAS NMR, X-ray Microanalysis and ICP-MS.

Attenuated total reflection/Fourier transform infrared (ATR/ FTIR) was used to confirm the formation of polymer on the PVDF-phob support. The ATR/FTIR spectra of the molecularly imprinted membrane (MIM) co-polymerised with EDMA and DMAEM, of the PVDF-phob support alone and of the pure EDMA are shown in figure 4. So, the spectrum a) is the PVDF-phob blank support, the spectra b) and c) correspond to the

DMAEM molecularly imprinted membrane after 10 minutes and 24 h of UV radiation, respectively. And the spectrum c) is the spectra of pure EDMA.

In the spectrum (a), the main band at 1200 cm^{-1} is the deflection vibration of C-H, C-C and C-F bonds. Between 1020 and 1330 cm^{-1} there are the bands of C-H and C-F. [57] between A 505 and 880 cm^{-1}, there are the *stretching* vibration of C, H and F atoms [58].

The most significant changes in the MIM spectra, in comparison with spectrum a), are the band at 1730 cm^{-1} corresponding to the carbonyl group. This band correspond both ester carbonyl of the EDMA and DMAEM. Other important bands are those at 1638 cm^{-1} and 950 cm^{-1} that indicate the presence of un-reacted free double bonds in the material. [59] These bands are of low intensity and can be attributed to the deposition of EDMA (not polymerised), or to the terminal groups of the polymer. The band at 1450 cm^{-1}, corresponding to $-O-CH_2$-bending, also confirms the polymerization over the PVDF-phob support. It is remarkable to observe that the spectrum c), corresponding to the MIM after 24 h of UV radiation, present a footprint more similar to the footprint of EDMA (spectrum d) than to the blank support (spectrum a). Thus, it may be stated that the molecularly imprinted polymer covers the major part of the surface of the support.

In order to determine the presence of the template L-selenomethionine in the imprinted polymer, ATR/FTIR was also used. In figure 5 the spectra of both membranes prepared with (a) and without (b) the template are shown. The main differences when the L-amino acid is used as template are: a more intense and wider band at 3400-3200 cm^{-1}, corresponding to N-H stretching vibration (st) (spectrum a), two bands at 1550 and 1595 cm^{-1} which correspond to NH_3^+ symmetric (sym) and COO^- (st) vibration, respectively [60,61]. All bands confirm the presence of the L-selenomethionine in the imprinted membrane.

For the same purpose, in order to assure the inclusion of the template in the membrane, X-ray microanalysis coupled to the scanning electron microscope was used, so to check the presence of selenium in the membrane surface corresponding spectra are shown in figure 6. The common bands of both spectra correspond to C and O that come from PVDF-phob material, and the Au which is from the sample pre-treatment. The only difference is the band of selenium that appears in the membrane polymerized in presence of the template L-selenomethionine. [62] It has to be note that Se band does not appear regularly through the entire membrane surface. Figure 7 illustrate the SEM image on which X-ray measurement was carried out. It is possible to distinguish between different zones where the selenium is or is not present. It seems that selenomethionine is deposited easily where the polymerization is crowd.

Also, the permeation water flux for some DMAEM-MIM in front of the pressure was determinated. Certain differences were found as a function of the polymerization time as it may be seen in figure 8. The flows rates of the imprinted membranes were higher than the flow rate of initial PVDF-phob support. Taking into account that the initial material is a hydrophobic support, this increase is found because the co-polymer introduced polar groups which increase the flux of water through. [63,64]

Further characterization of the polymer was conducted. The study of the polymer by high resolution NMR was not possible due to the insolubility of it in common NMR solvents. For this reason a preliminary study of the polymer synthesized with DMAEM as a monomer, as a solid sample, by ^{13}C CP/MAS NMR was carried out. Figure 9 shows the ^{13}C CP/MAS NMR spectra of (a) the PVDF-phob support, (b) the polymer synthesized without the presence of the support, and (c) the polymer synthesized on the PVDF-phob support. All the spectra were recorded at 298 K, at a spinning rate of 12

kHz and accumulated overnight. It may be observed that the spectrum of the latter (c) corresponds to the sum of (a) and (b), confirming the deposition of the polymer on the PVDF-phob support. There is no detectable chemical shift difference or change in line shape between the pure polymer and the polymer deposited on the support. In general, the resolution of the carbon polymer signals is quite poor, even though the samples were spun at 12 kHz and in a 400 MHz spectrometer. The low field signal at 177 ppm arises from the carbonyl carbons of the sample. High field signals (from 61 to 17 ppm) are poorly resolved, making difficult their assignment. However it could be assigned to –CH3 groups. [65] The assignment of the carbons of the PVDF-phob support is shown in figure 9.

The proper removal of the template, before using the MIMs, was confirmed by inductively coupled plasma mass spectroscopy (ICP-MS).

Simultaneously the analysis of the water solutions used for the template removal permit the quantification of L-selenomethionine in terms of $mg \cdot cm^{-2}$ in the membrane surface. Membranes with different degree of modification (DM) were compared by using 0,01 of L-selenomethionine in all cases. Figure 10 shows the influence of the DM on the amount of L-SeMet recovered. As it was expected, when the DM increases from 365 $\mu g \cdot cm^{-2}$ to almost 1000 $\mu g \cdot cm^{-2}$ the amount of template removed also increases, from 0,005 $mg \cdot cm^{-2}$ of until 0,01 $mg \cdot cm^{-2}$ L-Selenomethionine. So, in the case of approximately 3 hours of polimeritzation time, the amount of L-selenomethionine is ca. 0,2 mg, in membranes with 17,35 cm^2 of surface. This proves that the amount of L-selenomethionine imprinted corresponds to the 80 % of the initial amount. Therefore, it should be considered to use a lower L-selenomethionine amount to carry out the polymerization.

3.4 Enantioselective transport across DMAEM-MIM.

3.4.1. Effect of pH of the aqueous phases.

Three pH values 5, 6 and 8 were studied. All chemical forms of selenomethionine may be found within this pH range. At pH 5 selenomethionine is positively changed (amino group protonated, pKa = 9, 65); at pH 6 it is neutral in balance (zwitterionic form, isoelectric point, pI = 5,99); and at pH 8 it is negatively changed (deprotonated carboxylic group, pKa = 2,26). In the figure 11 the alpha factor values in front of the pH of the feed and the stripping phases are represented. At pH 5 practically no separation is found. On the other hand, at pH 6 and 8 the alpha factor is 1,75 and 1,35 respectively.

Taking into account that the tertiary amine of DMAEM is an important nucleophylic group, the main use of this monomer is to recognize acid templates or electrophylic groups. Thus, we could explain the bad enantiomeric separation at pH 5 because the amine group of the amino acid is protonated as well as the tertiary amine of DMAEM. In consequence, all the functional groups have electrophyl behaviour (even the carboxylic acid) so the possible interactions as hydrogen bonds or ionic bonds do not take place. The best enantioseparation was obtained at pH 6. A possible explanation for that may be related to the interaction between the carboxylate group of the amino acid and the protonated tertiary amine of DMAEM making an ionic bond, which is related to the zwitterionic structure of the aa at such pH. The decrease of the enantioseparation at pH 8 can be related to the decrease of the protonated amine form, becoming nucleophylic groups.

In figure 12, the selenomethionine re-extraction is shown, during 72 hours at pH 6. The transport by diffusion achieves the equilibrium after 24 hours and the D-selenomethionine is the enantiomer that moves more quickly across the membrane. It

means that the imprinted membrane is able to keep the L-enantiomer into the polymer structure and allows the transport of D-selenomethionine with a higher rate, in such conditions.

3.5.2. Effect of monomer and cross-linker concentration

With the aim to evaluate the effect of the monomer and cross-linker concentrations in the separation of the DL-selenomethionine, the concentration of them was changed to prepare the imprinted membranes. As shown in table 2, the concentration of monomer was varied from 0.01 to 0,135 M, while the cross-linker concentration was varied from 0,05 to 0,3 M. The flux ($\mu mols \cdot h^{-1} \cdot cm^{-2}$) at 24 h as well as the separation factor were calculated. Higher fluxes were obtained when the concentration of one or both of the components (cross-linker and monomer) was increased. Only when both concentrations were low, the fluxes of both enantiomers decreased, in certain cases, more than two orders of magnitude. This behaviour agrees with the water fluxes previously presented in figure 8: when the co-polymer concentration/amount increases, the flows increases due to the major presence of the hydrophilic groups.

The fluxes are defined as the decrease of matter of feed solution with time, t, and for unit area, A. In other words, it corresponds to the extraction's rate of the analytes from feed phase to membrane phase. As can be seen in table 2, the extraction of the enantiomers takes place without any separation because the difference between the enaniomers's fluxes is very little. As a foresaid, the process of enantioseparation is produced in the re-extraction step, when the L-selenomethionine is kept retained by and in the polymeric structure.

An important thing to note is that, when the fluxes increase, the separation of the enantiomers decreases. [66] In this way, higher alpha factors where obtained when the

fluxes of the enatiomers were less than 10^{-5} $\mu mols \cdot h^{-1} \cdot cm^{-2}$. The problem is that the amount of the analytes transported is very small and the time required is too large.

Finally, the variation of the template, L-selenomethionine, from 0, 01 to 0, 001 mg, during the preparation of the imprinted polymer did not affects significantly the separation factor. It is due to the fact that the L-selenomethionine concentration is in excess, as explained in section 3.3, figure 10.

4. Conclusions

Molecularly imprinted membranes (MIM) were synthesized for the first time, for the chiral separation of the D L-selenomethione. The use of conventional techniques as Scanning Electron Microscopy with X-Ray microanalysis (SEM) or Attenuated Total Reflection/Fourier Transform InfraRed (ATR/FTIR) allowed us to guarantee the presence of the polymer over the PVDF-phob support membrane. For the first time in MIM characterization, a preliminary study by ^{13}C CP/MAS NMR of the polymer synthesized with DMAEM as a monomer was carried out, allowing the detection of the co-polymer over the PFDV-phob support. This is an interesting technique for membranes characterization that would have to be studied in depth especially for the non soluble materials.

In terms of selectivity, the use of 100 mM of DMAEM as a monomer and 0,3 M of EDMA as a cross-linker in a water solution of pH 6 were the best conditions to obtain the highest chiral separation. The amount of the template L-selenomethionine necessary to prepare the imprinted membranes was 0,2 $mg \cdot cm^2$.

Although the molecularly imprinted membranes (MIM) is a young discipline in comparison of the molecularly imprinted polymers (MIP), the increase of contributions in that filed in the last decade are helping the evolution of MIM process. Little works

are focused in chiral separation, but the possibility to separate the enantiomers by membrane technology is able to become attractive, and the investigation has to be continued.

Acknowledgements

This work was supported by the C.I.C.Y.T. (Ref: PPQ2002-024201-C02-01, CTQ2005-09430-C05-01 and CTQ2004-02013). Aleix Conesa acknowledges the pre-doctoral fellowship from the *Departament de Química* of the *Universitat Autònoma de Barcelona* (Catalunya, Spain). The authors wish to thank the S*ervei de Microscopia Electrònica* of the *Universitat Autònoma de Barcelona UAB* (Catalunya, Spain) for the SEM analysis.

Figures

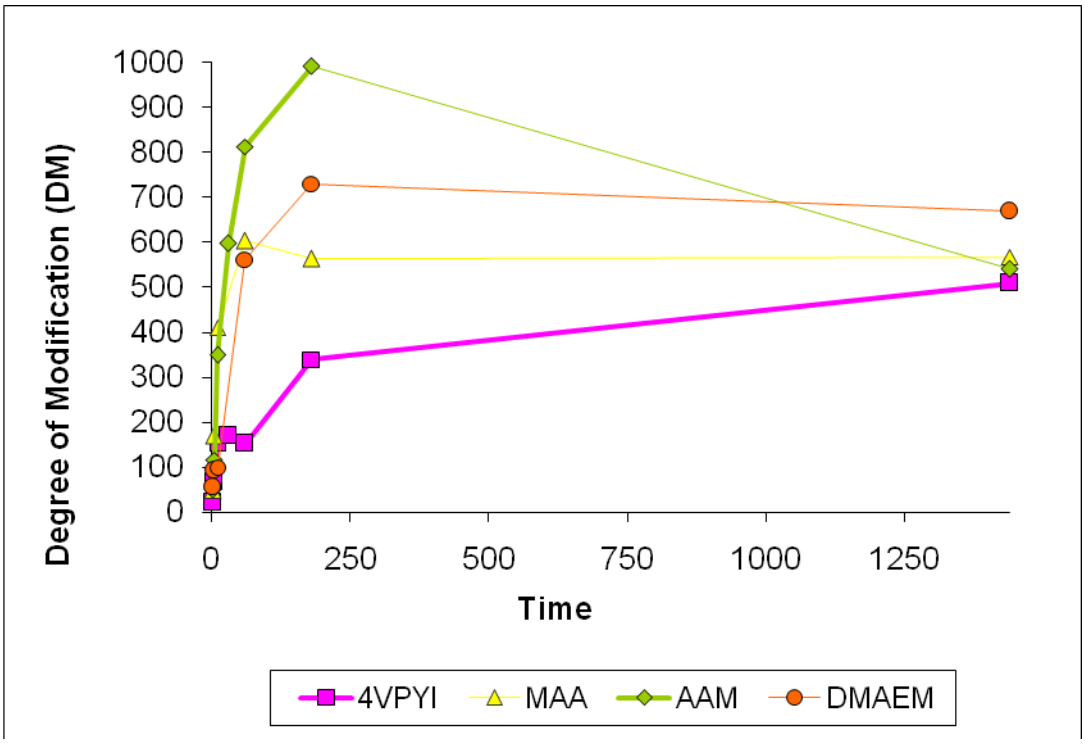

Figure 1. Degree of modification (DM) for the four monomers used: 4-vinylpiridine (4VPY), methacrylic acid (MAA), acrylamide (AAM) and N,N-dimethyl-2-aminoethylmethacrylate (DMAEM).

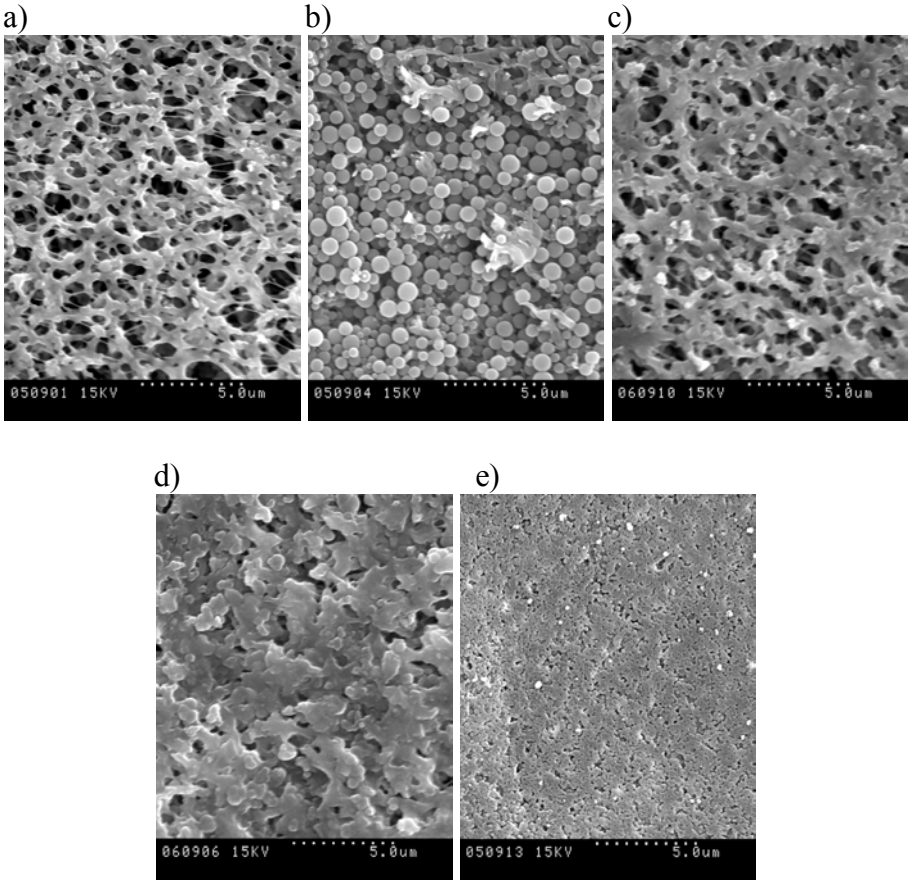

Figure 2. SEM surface images prepared with the monomers and co-polymerized with ethylene glycol dimethacrylate (EDMA): a) PVDF blank membrane b) 4-vinylpiridine (4VPY); c) methacrylic acid (MAA); d) acrylamide (AAM); e) N,N-dimethyl-2-aminoethylmethacrylate (DMAEM).

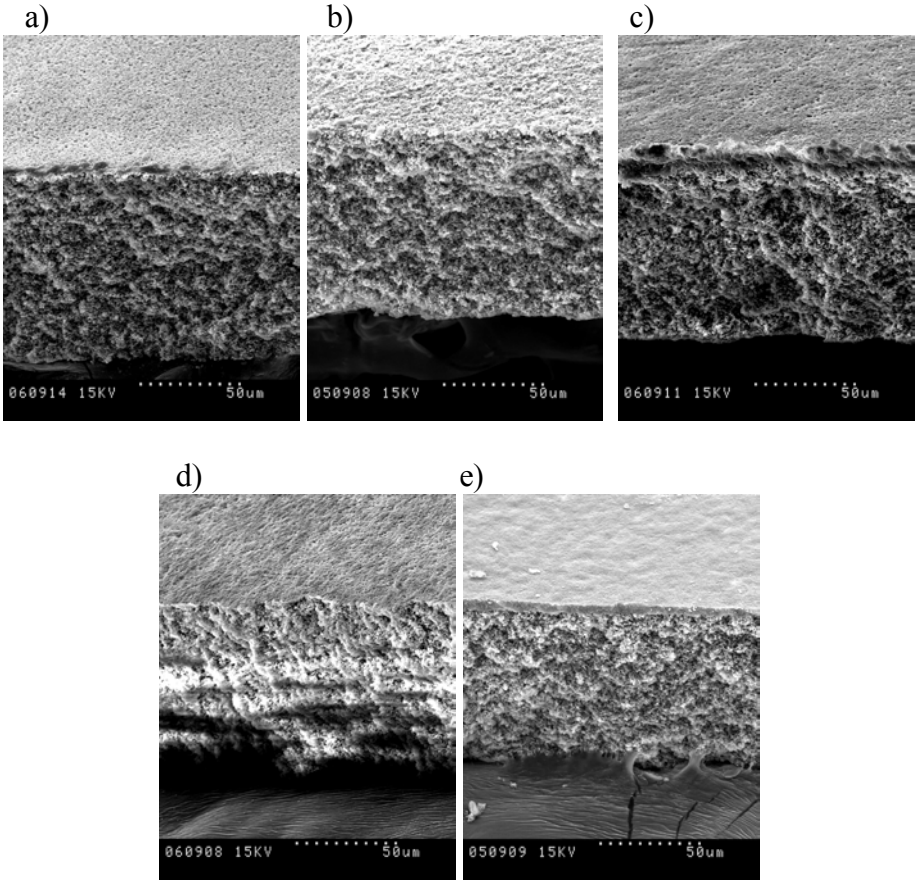

Figure 3. SEM cross-section images prepared with the monomers and co-polymerized with ethylene glycol dimethacrylate (EDMA): a) PVDF blank membrane b) 4-vinylpiridine (4VPY); c) methacrylic acid (MAA); d) acrylamide (AAM); e) N,N-dimethyl-2-aminoethylmethacrylate (DMAEM).

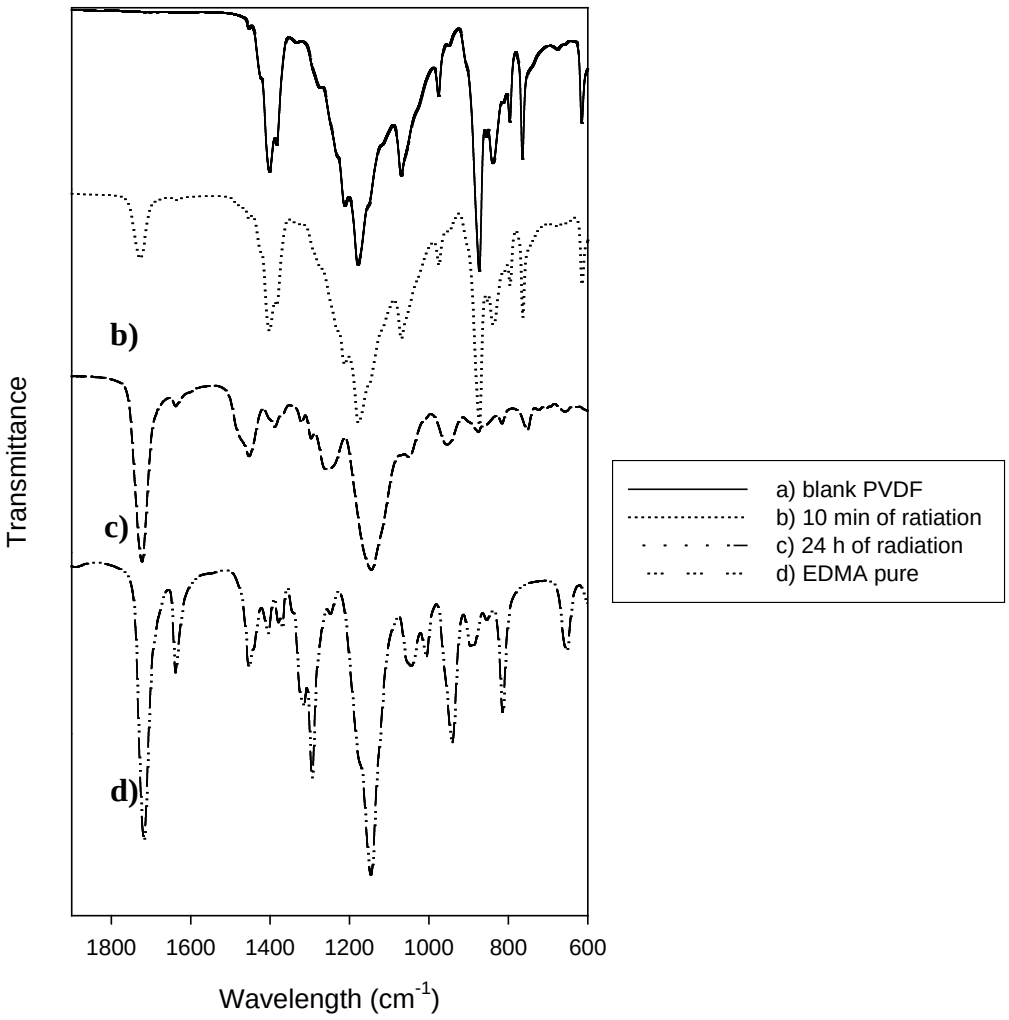

Figure 4. The spectra of the molecularly imprinted membranes (MIM) co-polymerised with EDMA and DMAEM at different times of radiation and PVDF-phob membrane without modification.

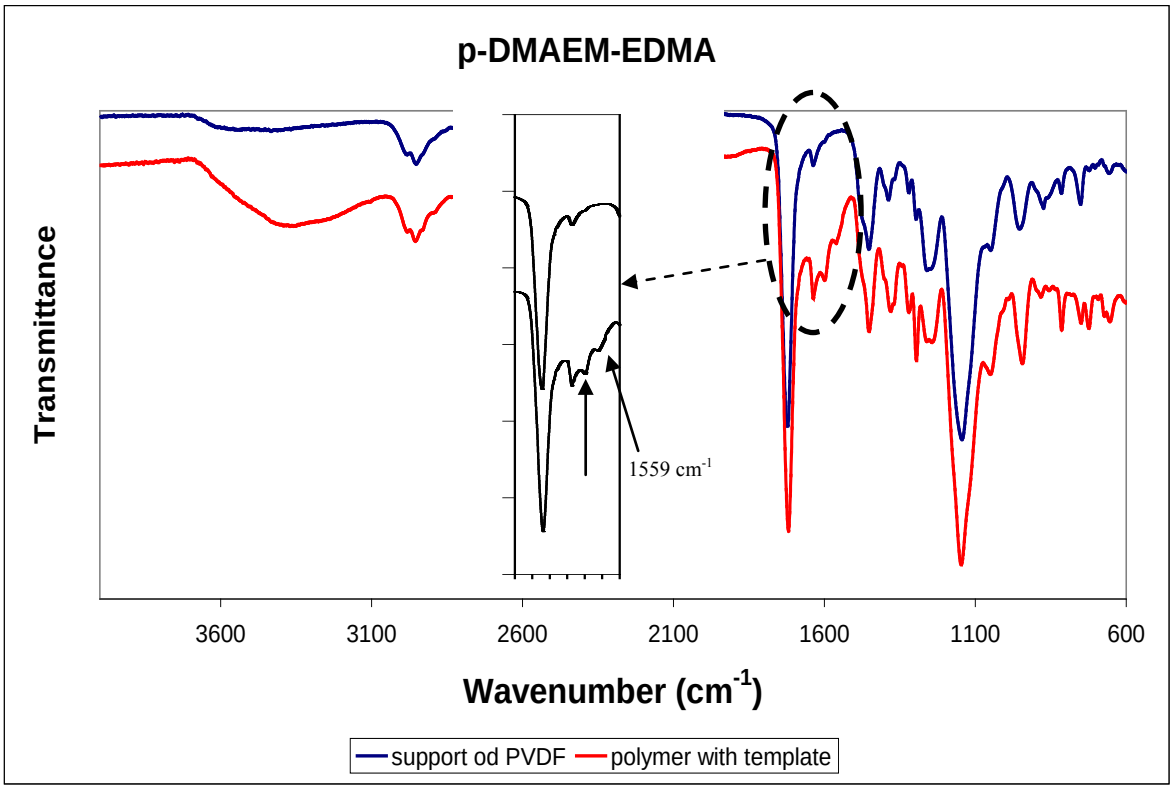

Figure 5. The spectra of a membrane prepared with the presence of the template (spectra a) and without the presence of this (spectra b).

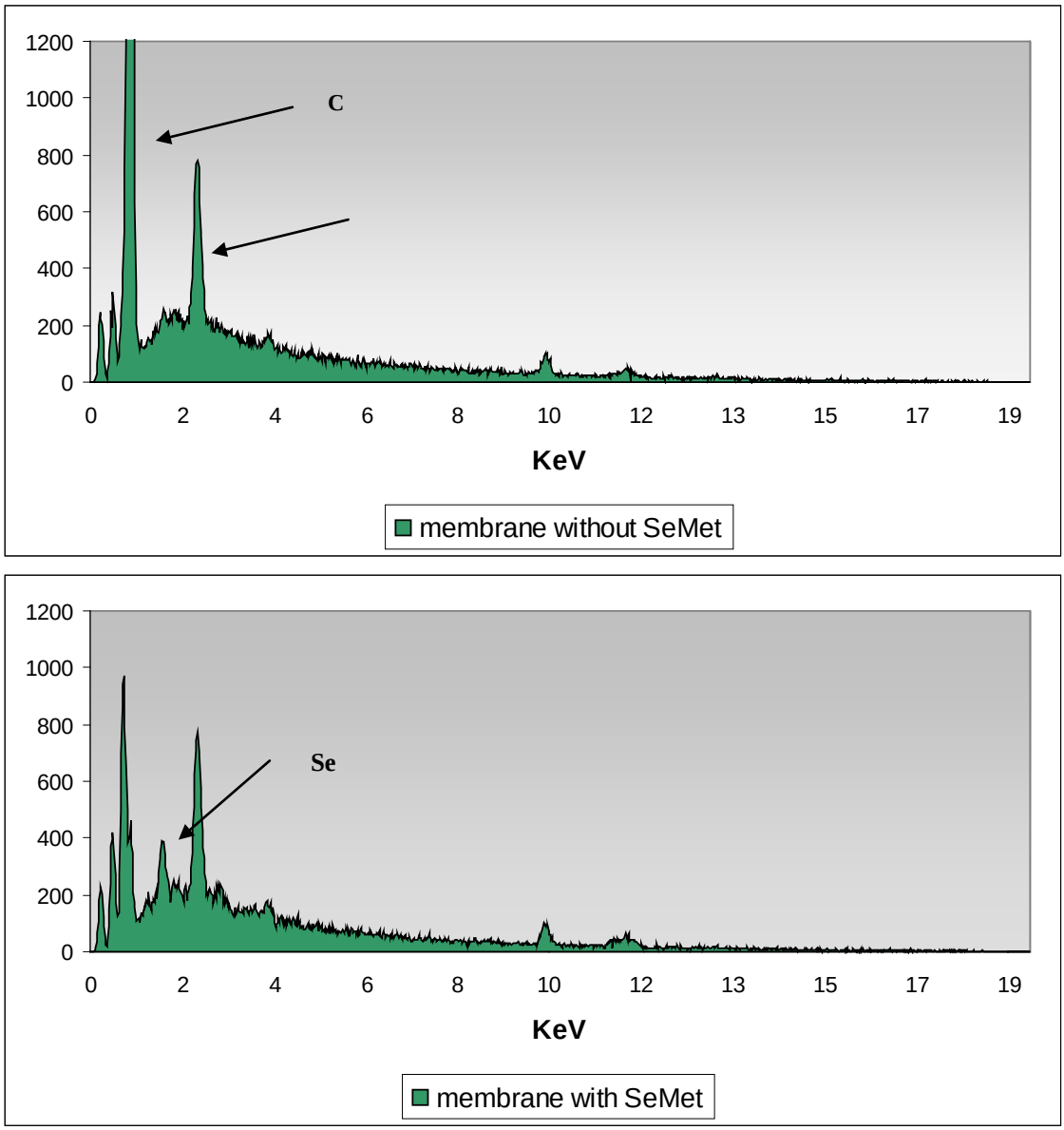

Figure 6. a) The spectra obtained by X-Ray microanalysis coupled to the scanning electron microscope. a) Membrane without Selenomethionine; b) Membrane with selenomethionine.

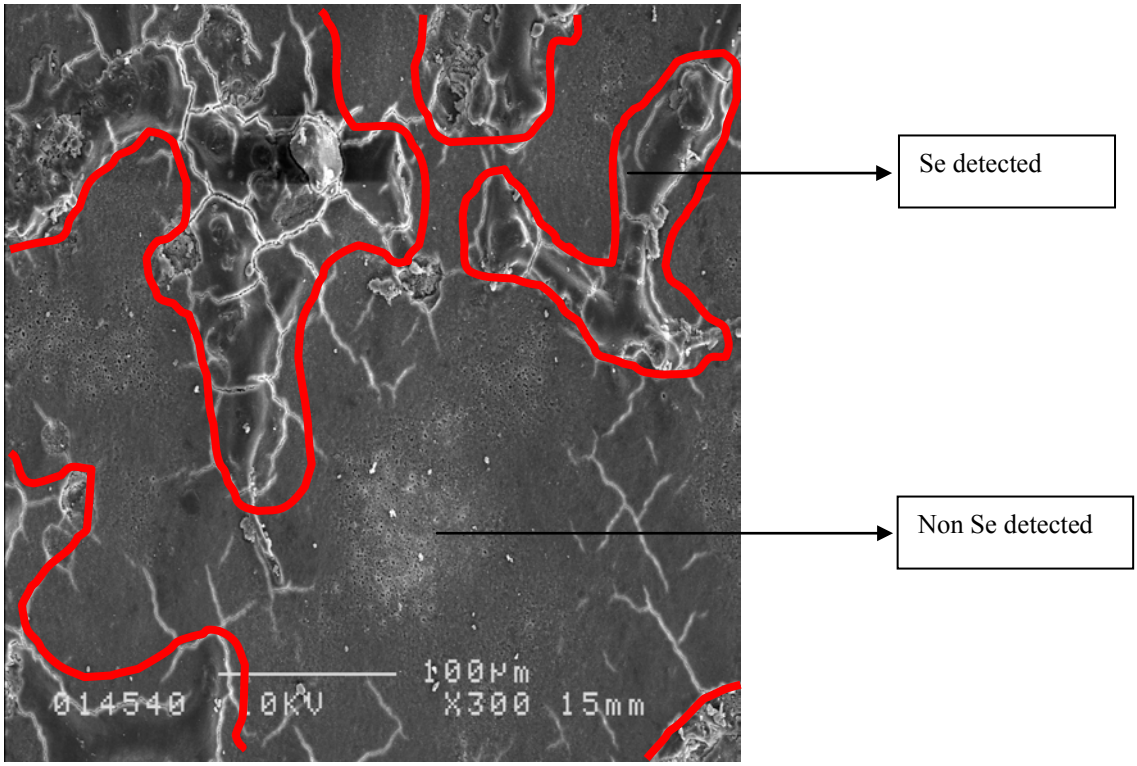

Figure 7. The SEM image where the X-ray was taken. It is mark the zones where the selenium was detected and in which no.

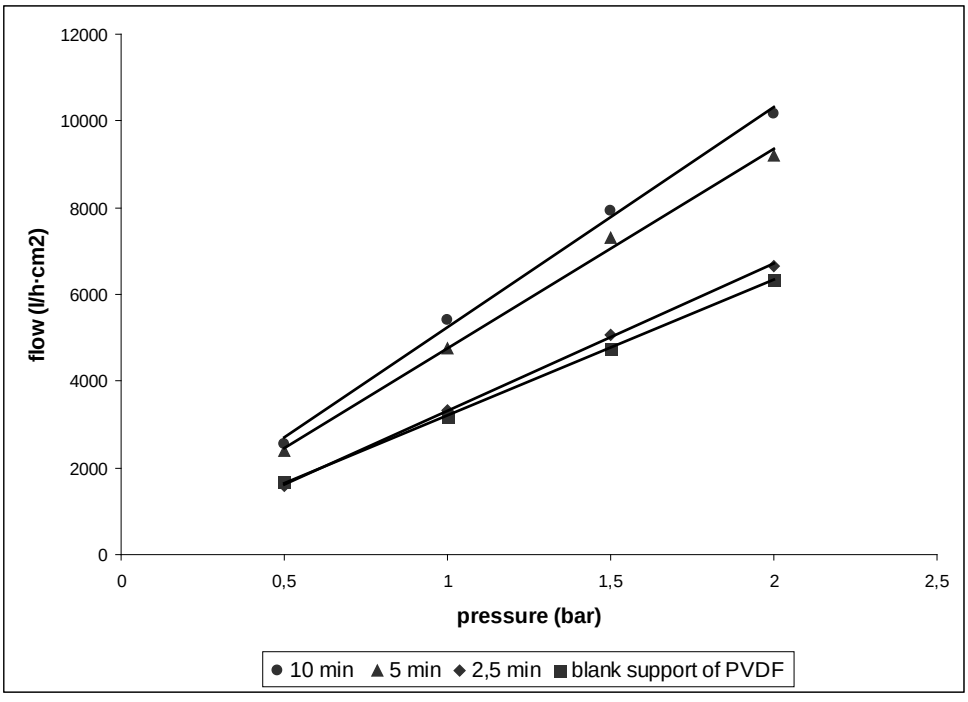

Figure 8. DMAEM-MIM water flow ($l/h^{-1} \cdot m^{-2}$) thought the imprinted membrane at different pressures.

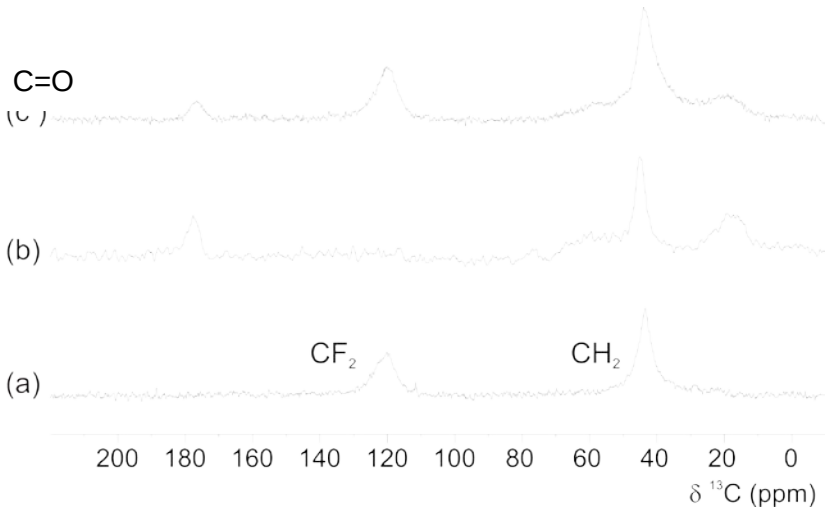

Figure 9. ^{13}C CP/MAS NMR of (a) the PVDF membrane, (b) the DMAEM polymer and (c) the DMAEM polymer deposited on the PVDF membrane; acquired at 12 kHz spinning rate and at 298 K.

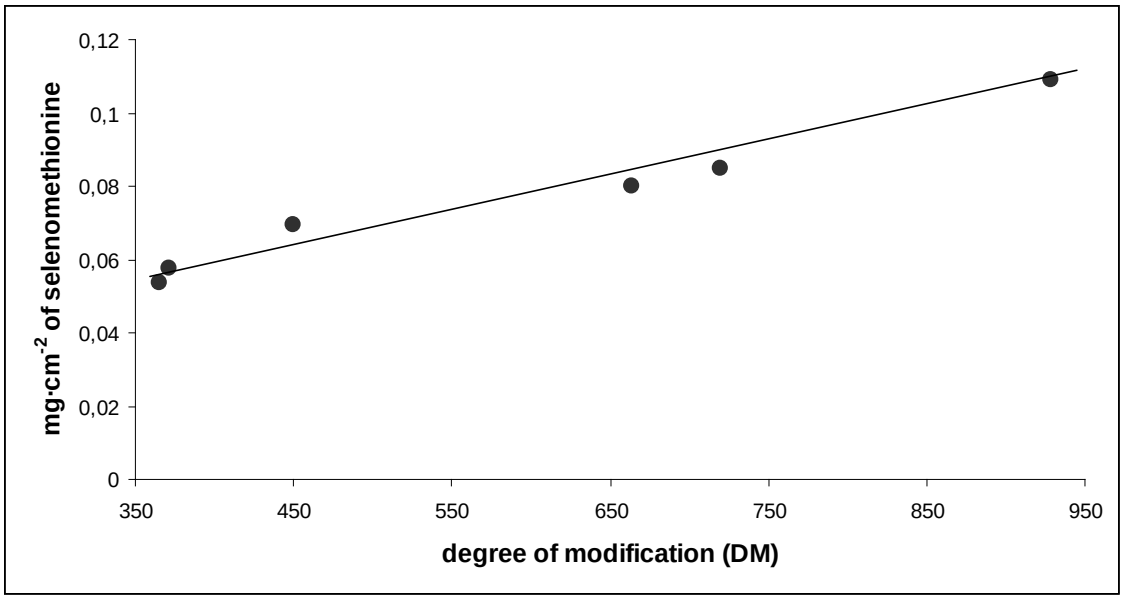

Figure 10. Relation between the DM and the amount of L-SeMet removed ($mg \cdot cm^{-2}$).

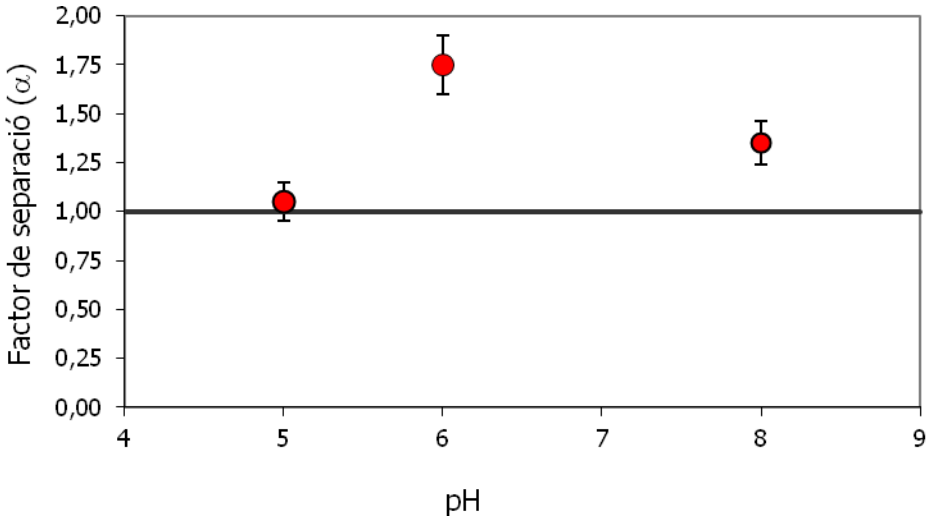

Figure 11. Separation factor (α) obtained in front of the pH using DAEM membrane.

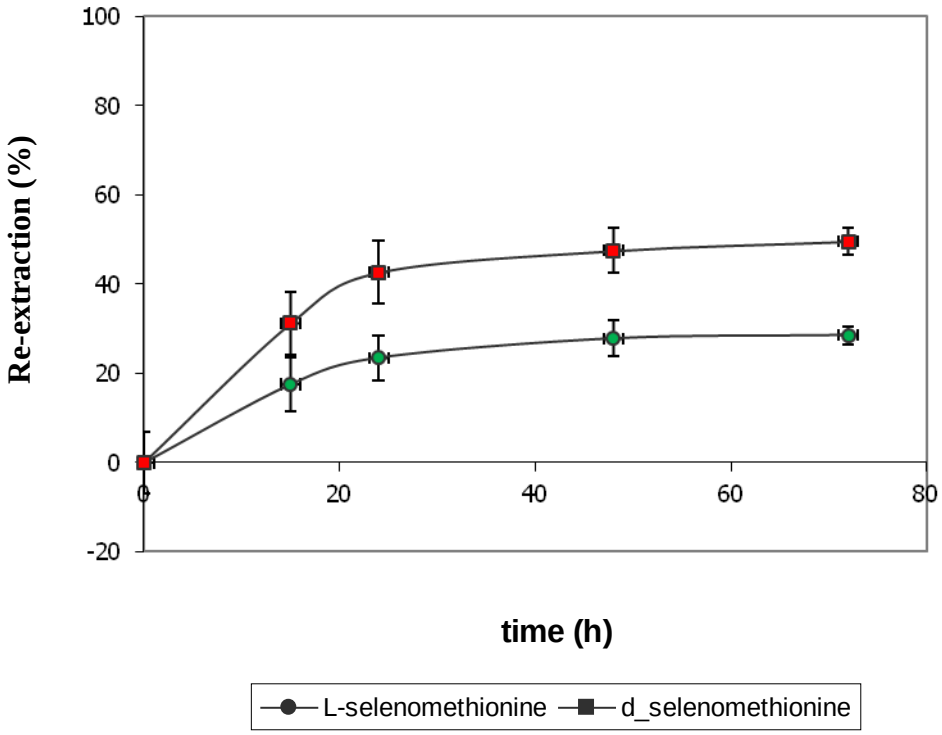

Figure 12. Re-extraction of L and D. Conditions: feed and stripping phases buffered at pH 6 and using DMAEM as a monomer.

Tables

Table 1

Monòmer	$\alpha_{D/L}$ membrana d'impressió	$\alpha_{D/L}$ membrana blanc
DMAEM	1,37 ± 0,09	1,06 ± 0,02
MAA	1,20 ± 0,06	1,03 ± 0,01
4-VYP	1,18 ± 0,05	0,97 ± 0,05
AAM	Sense separació quiral	

Table 2

EDMA (M)	DAEM (M)	J_L (µmols·h^{-1}·cm^{-2}) · 10^{-3}	J_D (µmols·h^{-1}·cm^{-2}) · 10^{-3}
0,0500	0,0200	0,0780	0,0360
0,0500	0,0200	0,235	0,0680
0,300	0,0200	0,589	0,517
0,275	0,135	0,853	0,889
0,0500	0,0100	2,59	2,43
0,0500	0,0100	2,98	2,73

References

[1] R. Abdulah, K. Miyazaki, M. Nakazawa and H. Koyama, Chemical forms of selenium for cancer prevention, Journal of trace Elements in Medicine and Biology, 19 (2-3) (2005) 141-150.

[2] D. Voet, J.G. Voet, Biochemistry, Wiley, New York, 1995.

[3] B. Sellergren, Molecularly imprinted polymers. Man-made mimics of antibodies and their applications in analytical chemistry, first edition by elsevier, Netherlands 2001.

[4] M.V. Polyakov, Adsorption properties and structure of silica gel. Zhur. Fiz. Khim., 2 (1931) 799-805.

[5] T. Takagishi and I.M. Klotz, Macromolecule-small molecule interactions; introduction of additional binding sites in polyethyleneimine by disulfide cross-linkages. Biopolymers, 11 (1972) 483-491.

[6] G. Wulff and A. Sarhan, The use of polymers with enzyme-analogous structures for the resolution of racemates. Angew. Chem., 11 (1972) 341. Intl. Ed. Engl. 11: 341.

[7] K. Mosbach, Molecular imprinting. Trends Biochem. Sci. 19 (1994) 9-14.

[8] S.A. Piletsky, T.L. Panasyuk, E.V. Piletskaya, I.A. Nicholls and M. Ulbricht, Receptor and transport properties of imprinted polymer membranes – a review, J. of Membrane Science, 157 (2007) 263-278.

[9] M. Ulbricht, Membrane separation using molecularly imprinted polymers, J. of Chromatography B, 804 (2004) 113-125.

[10] T. Kobayashi, H. Y. Wang and N. Fujii, Molecular imprinted membranes of polyacrylonitrile copolymers with different acrylic acid segments, Analytica Chimica Acta, 365 (1998) 81-88.

[11] P. S. Reddy, T. Kobayashi, M. Abe and N. Fujii, Molecular imprinted Nylon-6 as a recognition material of amino acids, European Polymer Journal, 38 (2002) 521-529.

[12] M. Ramamoorthy and M. Ulbricht, Molecular imprinting cellulose acetate-sulfonated polysulfone blend membranes for Rhodamine B by phase inversion technique, Journal of Membrane Science, 217 (2001) 201-214.

[13] E. Trotta, C. Baggiani, M.P. Luda, E. Drioli and T. Massari, A molecular imprinted membrane for molecular discrimination of tetracycline hydrochloride, Journal of Membrane Science, 254 (2005) 13-19.

[14] M. Ulbricht and R. Malaisamy, Insights into the mechanism of molecular imprinting by immersion precipitation phase inversion of polymer blands via a detail morphology analysis of porous membranes, Journal of Materials Chemistry, 15 (2005) 1487-1497.

[15] Y. Hu, J. Pan, K. Zhang, H. Lian, G. Li, Novel applications of molecularly-imprinted polymers in sample preparation, TrAC-Trend. Anal. Chem., 43 (2013) 37-52.

[16] J. Mathew-Krotz and K.J. Shea, Imprinted Polymer for the Selective Transport of Target Neutral Molecules, J. Am. Chem. Soc., 118 (1996) 8154-8155.

[17] S.A. Piletsky, H. Matuschewski, U. Schedler, A. Wilpert, E. V. Piletska, T. A. Thiele and M. Ulbricht, Surface Functionalization of Porous Polypropylene Membranes with Molecularly Imprinted Polymers by Photograft Copolymerization in Water, Macromolecules, 33 (2000) 3092-3098.

[18] F. Trotta, E. Drioli, C. Baggiani and D. Lacopo, Molecular imprinted polymeric membrane for naringin recognition, 201 (2002) 77-84.

[19] R. Song, X. Hu, P. Guan, J. Li, N. Zhao, Q. Wang, "Molecularly imprinted solid-phase extraction of glutathione from urine samples", Mater. Sci. Eng. C, 44 (2014) 69-75.

[20] K. Schwarz and C.M. Foltz, Selenium as an integral part of factor 3 against dietary necrotic liver degeneration. J. Am. Chem. Soc. 79 12 (1957) 3292-3293.

[21] J.T. Rotruck, H.E. Ganther, A.B. Swanson, D.G. Hafeman, and W.G. Hoekstra. Selenium: biochemical role as a component of glutathione peroxidase, Science, 179 (1973) 588-590

[22] M.C.C. Perez, A.L. Latorre, M.J.A. López, J.M.L. Vilariño, M.V.G. Rodríguez, A study competitive molecular interaction effects on imprinting of molecularly imprinted polymers, Vib. E spectrosc., 65 (2013) 74-83

[23] V.L.V. Granado, A. Rudnitskaya, J.A.B.O. Oliveira, M.T.S.R. Gomes, Design of molecularly imprinted polymers for diphenylamine sensing, Talanta, 94 (2012) 133-139.

[24] T. Hjertberg, 13C CP-MAS NMR Study on Content and Mobility of Double Bonds in Poly(trimethylpropane trimerhacrylate), Macromolecules, 23 (1990) 3080-3087.

[25] R. V. Law, D. C. Sherrington abd C. E. Snape, Solid-Sate 13C MAS NMR Studies of Hyper-Cross-Linked Polystyrene Resins, Macromolecules, 29 (1996) 6284-6293.

[26] J. Courtois, G. Fisher, S. Schauff, K. Albert and K. Irgum, Interactions of Bupivacaine with a Molecularly Imprinted polymer in a Monolithic Format Studied by NMR, Anal. Chem., 78 (2006) 580-584.

[27] U. Skogsberg, C. Meyer, J. Rehbein, G. Fischer, S. Schauff, N. Welsch, K. Albert, A. J Hall, B. Sellergren, A solid-state suspended-state magic angle spinning nuclear magnetic resonance spectroscopic investigation of a 9-ethyladenine molecularly imprinted polymer, Polymer, 48 (2007) 229-238.

[28] B. Rückert, U. Kolb, "Distribution of molecularly polymer layers on macroporous silica gel particles by STEM and EDX", Micron, 36 (2005) 247-260.

[29] S.A. Kosa, I.H.A. El Maksod, L. Alkheteeb, E.Z. Hegazy, "Preparation and surface characterization of CuO and Fe2O3 catalyst", Appl. Surf. Sci., 258 (19) (2012) 7617-7624.

[30] G. H. Lyons, G. J. Judson, I. Ortiz-Monasterio, Y. Genc, J. C.R. Stangoulis and R. D. Graham, Selenium in Australia: Selenium statusand biofortification of wehat for better health, J. of Trace Elements in Medicine and Biology, 19 (2005) 75-82.

[31] D. H. R. Barton, D. Bridon, Y. Hervé, P. Potier, J. Thierry and S. Z. Zard, Concise syntheses of L-selenomethionine and L-selenocystine using radical chain reactions, Tetrahedron, 42 (1986) 4983-4990.

[32] T. Koch and O. Buchardt, Synthesis of L-(+)-selenomethionine, Synthesis, 11 (1993) 1065-1067.

[33] G.N. Schrauzer, Selenomethionine and selenium yeast: appropriate forms of selenium for use in infant formulas and nutritional supplements, J. Med. Foods, 1 (1998) 201–206.

[34] V. Kochkodan, W. Weigel and M. Ulbricht, Thin layer moleculary imprinted microfiltration membranes by photofunctionalization using a coated a-cleavage photoinitiator, Analyst, 126 (2001) 803-809.

[35] T. A. Sergeyeva, H. Matuschewski, S. A. Piletsky, J. Bending, U. Schedler and M. Ulbricht, Molecularly imprinted polymer membranes for substance-selective solid-phase extraction from water by surface photo-grafting polymerization, J. of Chromatogr. A, 907 (2001) 89-99.

[36] A. Dzgoev and K. Haupt, Enantioselective Molecularly Imprinted Polymer Membranes, Chirality, 11 (1999) 465-469.

[37] S. Pérez Méndez, E. Blanco González and A. Sanz Medel, Chiral speciation and determination of selenomethionine en antiomers in selenized yeast by HPLC-ICP-MS using a teicoplanin-based chiral stationary phase, J. Anal. At. Spectrom., 15 (2000) 1109-1114. DOI: 10.1039/b001579m.

[38] N. Hilal and V. Kochkodan, Surface modified microfiltration membranes with molecularly recognising properties, Journal of Membrane Science, 213 (2003) 97-113.

[39] N. Hilal, V. Kochkodan, G. Busca, O. Kochkodan, B.P. Atkin, "Thin layer composite molecularly imprinted membranes for selective separation of cAMP", Sep. Purif. Technol., 31 (2003) 281-289.

[40] D.T. Landin and C. W. Macosko, Cyclization and Reduced Reactivity of Pendant Vinyls during the Copolymerization of Methyl Methacrylate and Ethylene Glycol Dimethacrylate, Macromolecules, 21 (1988) 846-851.

[41] W.-H. Li, A. E. Hamielec and C.M. Crowe, Kinetics of the free-radical copolymerization of methyl methacrylate/ethylene glycol dimethacrylate: 1. Experimental investigation, Polymer, 30 (1989) 1513-1517.

[42] K. Samba Sivudu, S. Thomas, D. Shailaja, Synthesis and characterization of poly(4vp-co-dvb)/montmorillonite nanocomposites by in situ intercalative polymerization, Appl. Clay Sci., 37 (2007) 185-192.

[43] Y. Sueyoshi, A. Utsunomiya, M. Yoshikawa, G.P. Robertson, M.D. Guiver, Chiral separation with molecularly imprinted polysulfone-aldehyde derivatitzed nanofiber membranes, J. Membr. Sci., 401-402 (2012) 89-96.

[44] Y. Sueyoshi, C. Fukushima, M. Yoshikawa, Molecularly imprinted nanofiber membranes from cellulose acetate aimed for chiral separation, J. Membr. Sci., 357 (2010) 90-97.

[45] M. Yoshikawa, T. Fujisawa, J.I. Izumi, T. Kitao, S. Sakamoto, Molecularly imprinted polymeric membranes involving tetrapeptide EQKL derivatives as chiral-recognition sites toward amino acids, Anal. Chim. Acta, 365 (1998) 59-67.

[46] C. Yu and K. mosbach, Molecular Imprinting Utilizing an Amide Functional Group for Hydrogen Bonding Leading to Highly Efficient Polymers, J. Org. Chem., 62 (1997) 4057-4064.

[47] R. Levi, S. McNiven, S. A. Piletsky, S.-H Cheong, K. Yano and I. Karube, Optical Detection of Chloramphenicol Using Molecularly Imprinted Polymers, Anal. Chem., 69 (1997) 2017-2021.

[48] S.A. Pilestsky, E.V. Pilestskaya, T.L. Panasyuk, A.V. El'skaya, R. Levi, I. Karube and G. Wulff, Imprinted Membranes for Sensor Technology: Opposite Behavior of Covalently and Noncovalently Imprinted Membranes, Macromolecules, 31 (1998) 2137-2140.

[49] S.A. Piletsky, Y.P. Parhometz, N.V. Lavryk, T.L.Panasyuk and A.V. El'skaya, Sensors for low-weight organic molecules based on molecular imprinting technique, Sens. Actuators B, 19 (1994) 629-631.

[50] C.Y. Xin, G-B. Jiao, J.H. Ming, Z.R. Xia, Constituting Chiral Caves by Using Novel Surface-Moleular Imprinting Technique and Realizating Chiral Separation of Enantiomers of Amino Acid; Acta Chim. Sinica, 69 (14) (2011) 1705-1714.

[51] J. Haginaka, H. Takehira, K. Hosoya and N. Tanaka, Molecularly Imprinted Uniform-Sized polymer Stationary Phase for Naproxen, Chem. Lett., 26 (1997) 555-556

[52] W. Chi, H. Shi, W. Shi, Y. Guo, T. Guo, 4-Nitrophenol surface molecularly imprinted polymers based on multiwalled carbon nantubes for elimination of paraoxon pollution, J. Hazard. Mater., 227-228 (2012) 243-249.

[53] G. Jianfeng, G. Baojiao, Studies on realizating chiral separation of enantiomers of aspartic acid by constituting chiral caves with surface–molecular imprinting technique, Acta Polym. Sinica, 1 (1) (2012) 47-55.

[54] B. Sellergren, Polymer- and template-related factors in£uencing the ef¢ciency in molecularly imprinted solid-phase extractions, Trends Anal. Chem., 18 (1999) 164-174.

[55] S. Asman, S. Mohamad, N.M. Sarih, Exploiting B-Cyclodextrin in Molecular Imprinteing for Achieving Recognition of Benzylparaben in Aqueous Media, J. Mol. Sci., 16 (2) (2015) 3656-3676.

[56] Y.M. Liu, C.Y. Lü, X. Fan, Z.P. Gao, Synthesis and Evaluation of Molecularly Imprinted Polymers Using Acetylsalicylic Acid as Template, J. Instrum. Anal., 26 (2) (2007) 165-169

[57] M. A. Masuelli, M. Grasselli, J. Marchese, N.A. Ochoa, Preparation, structural and functional characterization of modified porous PVDF membranes by g-irradiation, J. Membr. Sci., 389 (2012) 91-98.

[58] C.L. Wang, J.C. Li, W.L. Zhong, P.L. Zhang, IR vibrational Modes of PVDF chains, Synth. Met., 135-136 (2003) 469-470.

[59] K.J. Shea, G.J. Stoddard, D.M. Shavelle, F. Wakui and R.M. Choate, Syntesis and Characteritzation of Highly Cross-linked Polyacrylamides and Polymethacrylamides. A New Class of Macroporus Polyamides, Macromolecules, 23 21 (1990) 4497-4507.

[60] K. Löbmann, R. Laitinen, C. Strachan, T. Rades, H. Grohganz, Amino acids as co-amorphous stabilizers for poorly water-soluble drugs – Part 2: Molecular interactions, European J. Pharm. Biopharm., 85 (2013) 882-888.

[61] S. Suwal, C. Roblet, J. Amiot, L. Bazinet, Presence of free amino acids in protein hydrolysate during electroseparation of peptides: Impact on system efficiency and membrane physicochemical properties, Sep. Purif. Technol., 147 (2015) 227-236.

[62] Y.Y. Gurkan, E.Kasapbasi, Z. Cinar, Enhanced solar photocatalytic activity of TiO2 by selenium (IV) ion-doping: Characterization and DFT modeling of surface, Chem. Eng. J., 214 (2014) 34-44.

[63] Q. Cheng, Y. Zheng, S. Yu, H. Shu, X. Peng, J. Liu, J. Li, M. Liu, C. Gao, "Surface modificaction of a commercial thin-film composite polyamide reverse osmosis membrane through graft polymerization of N-isopropylacrylamide followed by acrylic acid", J. Membr. Sci., 447 (2013) 236-245.

[64] G.D. Kanh, Y.M. Cao, "Application of poly(vinylidene fluoride) (PVFD) membranes – A review", J. Membr. Sci., 463 (2014) 145-165.

[65] S.K. Tsermentseli, P. Manesiotis, A.N. Assimopuolou, V.P. Papageorgiou, Molecularly imprinted polymers for isolation of bioactive naphtoquinones from plant extracts, J. Chromatogr. A., 1315 (2013) 15-20.

[66] T. Gumí, M. Valiente, C. Palet, Elucidation of SR-propranolol transport rate and enantioselectivity through chiral activated membranes, Journal of Membrane Science, 256 (2005) 150-157.